arXiv:0807.2535v4 [physics.atom-ph] 7 Apr 2009

Ionization of Rydberg atoms by blackbody radiation

I.I. Beterov[1]§, D.B. Tretyakov[1], I.I. Ryabtsev[1], V.M. Entin[1], A. Ekers[2], N.N. Bezuglov[3]

[1]Institute of Semiconductor Physics, Pr. Lavrentyeva 13, 630090 Novosibirsk, Russia
[2]University of Latvia, Laser Centre, LV-1002 Riga, Latvia
[3]St. Petersburg State University, Faculty of Physics, 198904 St.-Petersburg, Russia

Abstract.

We have studied ionization of alkali-metal Rydberg atoms by blackbody radiation (BBR). The results of theoretical calculations of ionization rates of Li, Na, K, Rb and Cs Rydberg atoms are presented. The calculations have been performed for nS, nP and nD states for principal quantum numbers n=8-65 at ambient temperatures of 77, 300 and 600 K. The calculations take into account the contributions of BBR-induced redistribution of population between Rydberg states prior to photoionization and field ionization by extraction electric field pulses. The obtained results show that these phenomena affect both the magnitude of the measured ionization rates and their n-dependence. A Cooper minimum for BBR-induced transitions between bound Rydberg states of Li has been found. The calculated ionization rates are compared with our earlier measurements of BBR-induced ionization rates of Na nS and nD Rydberg states with n=8-20 at 300 K. A good agreement for all states except nS with $n > 15$ is observed. Useful analytical formulas for quick estimates of BBR ionization rates of Rydberg atoms are presented. Application of BBR-induced ionization signal to measurements of collisional ionization rates is demonstrated.

PACS numbers: 32.80.Fb, 32.80.Rm, 32.70.Cs

§ To whom correspondence should be addressed (beterov@isp.nsc.ru)

Contents

1. INTRODUCTION

Studies of blackbody radiation (BBR) started when Robert Kirchhoff noticed that BBR is of great importance in physics. The results of those studies facilitated the development of quantum mechanics. Today, after more than hundred years since its discovery, the blackbody radiation is important and interesting for researchers working in various areas of physics. The studies of BBR have revealed a number of new effects, for example anisotropy in the cosmic background radiation [1].

The most straightforward way to observe the interaction of BBR with matter relies on the use of atoms in highly excited Rydberg states with the principal quantum number $n \gg 1$ [2]. Rydberg atoms have many unique properties including large geometric size $\sim n^2$, large radiative lifetimes $\sim n^3$, large polarizabilities $\sim n^7$ and relatively low frequencies of transitions between neighboring states $\sim n^{-3}$. Since the dipole moments of low-frequency transitions between Rydberg states are very large, Rydberg atoms are extremely sensitive to electromagnetic fields, including the BBR. The studies of interaction of BBR with Rydberg atoms were initiated by Gallagher and Cooke in 1979 [2]. The authors of that pioneering work demonstrated that the influence of BBR must be taken into account in lifetime measurements, spectroscopy, and all other measurements where population of Rydberg states is monitored.

In the 1980-s, the interaction of Rydberg atoms with blackbody radiation was studied in various contexts. The attention was mainly focused on calculations and

measurements of lifetimes of Rydberg states [3–8] and BBR-induced Stark shifts [2, 9]. However, only a few studies considered ionization of Rydberg atoms by BBR. Interaction of a Rydberg atom A(nL) with the principal quantum number n and the orbital momentum L with BBR leads not only to transitions to other bound states, but also to transitions to the continuum:

$$\mathrm{A}\,(nL) + \hbar\omega_{BBR} \rightarrow \mathrm{A}^{+} + e^{-}. \tag{1}$$

Here, $\hbar\omega_{BBR}$ is the energy of the absorbed BBR photon, A^{+} is an atomic ion and e^{-} is a free electron emitted due to the ionization.

The first study of ionization of Rydberg atoms was published by Spencer et al. [10]. They calculated and measured the dependence of the sodium $17D$ BBR-induced photoionization rate on the ambient temperature. This study was followed by numerical calculations of BBR-induced ionization rates of H and Na atoms for a wide range of principal quantum numbers by Lehman [11]. In 1986, Burkhardt et al. [12] studied collisional ionization of Na Rydberg atoms. They concluded that BBR-induced ionization is the main mechanism of the atomic ion production. They also noticed that state-mixing collisions affect the dependences of the measured ionization rates on the principal quantum number. After an almost decade long pause the studies of interaction of Rydberg atoms with BBR were resumed by Galvez et al., who investigated the multistep transitions between Rydberg states caused by BBR [14] and the BBR-induced resonances between Rydberg states of Na in static electric fields [15]. A few years later, Hill et al. published a paper discussing the influence of the applied electric field on collisional and BBR-induced ionization rates of potassium Rydberg atoms [13].

Ionization of Rydberg atoms by BBR returned to the focus of researchers in 2000 in connection with the observation of spontaneous evolution of ultracold Rydberg atoms with $n > 30$ into an ultracold plasma initiated by BBR [16]. The creation of ultracold neutral plasma by laser photoionization of laser-cooled xenon atoms was reported by Killian et al. in 1999 [17]. Numerous studies of ultracold plasma followed immediately [18–28]. The ultracold plasma is an example of a strongly coupled plasma (the thermal energy of particles is less than the Coulomb interaction energy), which is substantially different from the ordinary high temperature plasmas. Strongly coupled plasmas appear in astrophysical systems, but are rather difficult to obtain in the laboratory.

The mechanism of spontaneous formation of ultracold plasma was described in [19]. After laser excitation, cold Rydberg atoms are ionized by blackbody radiation and by collisions with the hot Rydberg atoms. The produced electrons quickly leave the volume of a magneto-optical trap, but the cold ions do not. Then the macroscopic positive charge of the ions attracts and traps the electrons, making them oscillate back and forth through the cloud of cold Rydberg atoms. Collisions of electrons with the remaining Rydberg atoms lead to their rapid avalanche ionization. The electrons are thermalized to typical temperatures of tens of K, making such type of plasma really ultracold. The energy balance in the system is maintained by collisional depopulation of highly excited Rydberg states.

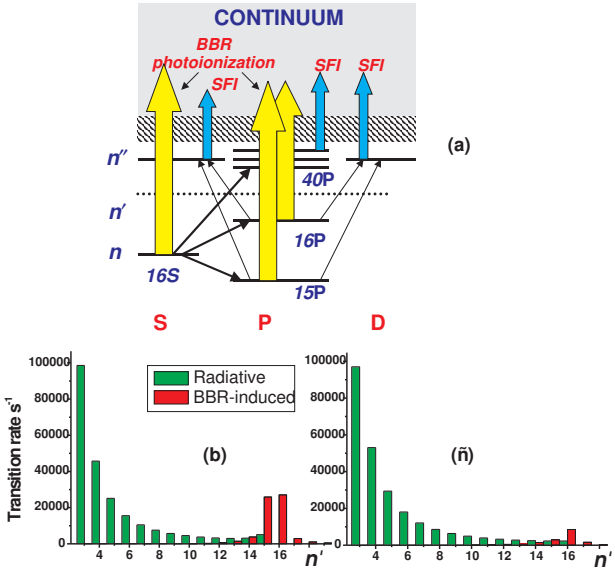

Figure 1. (a) Schematic illustration of BBR-induced and field ionization processes occurring after excitation of the initial Na(16S) state, including redistribution of population over other $n'L'$ Rydberg states due to spontaneous and BBR-induced transitions from the initial state. Highly excited $n''S$, $n''P$ and $n''D$ Rydberg states are ionized by the extracting electric pulses due to selective field ionization (SFI) [30]. (b) Calculated spontaneous and BBR-induced transition rates from the initial 16S state to other $n'P$ states. (c) Calculated spontaneous and BBR-induced transition rates from the initial 16D state to other $n'P$ states.

The estimates of BBR ionization rates in [16] were based on a simple analytical formula presented by Spencer et al. [10], which is a generalization of the results, obtained for Na 17D state. In the recent work [19] a simple approximation for photoionization cross-sections was used to calculate the BBR-induced ionization rate. The photoionization cross-section was expressed only through the energy of the Rydberg state and the energy of the absorbed photon, neglecting the specific properties of alkali-metal Rydberg states with low orbital momenta. Therefore, an extended systematic study of BBR-induced ionization of alkali-metal Rydberg atoms is required.

Another possible application of BBR-induced ionization is the correct measurement of collisional ionization rates of Rydberg atoms. In such experiments [29] a BBR ionization signal can be used as a reference for the determination of collisional ionization rate constants.

In the present work we discuss the mechanism of BBR-induced ionization of alkali-metal Rydberg atoms with low orbital momenta under realistic experimental conditions. The existing theoretical approaches are analyzed and compared. The simplest (but often insufficient) way of considering the BBR-induced ionization after the excitation of an atom A to a given nL Rydberg state is to take into account only the direct photoionization.

In the reality, however, ionization of Rydberg atoms exposed to BBR is a complex

process, in which the following main components can be identified [see figure 1(a)]: (i) direct photoionization of atoms from the initial Rydberg state via absorption of BBR photons, (ii) selective field ionization (SFI) [30] by extraction electric field pulses of high Rydberg states, which are populated via absorption of BBR photons by atoms in the initial Rydberg state, (iii) direct BBR-induced photoionization of atoms from the neighboring Rydberg states, which are populated due to absorption and emission of BBR photons prior to the photoionization, and (iv) field ionization of other high-lying states, which are populated via population redistribution involving two or more steps of BBR photon absorption and/or emission events. Our calculations show that all these processes can contribute to the total ionization rate to a comparable extent, and, therefore, none of them can be safely disregarded. In Section 2 we will consider the above processes and calculate the total BBR ionization rates, both analytically and numerically.

We present the results of numerical calculation of BBR-induced ionization rates for nS, nP and nD states of Li, Na, K, Rb and Cs atoms for a wide range of principal quantum numbers n=8-65 [31–33]. We also present simple analytical formulas for quick estimates of BBR-induced ionization rates. A Cooper minimum in the discrete spectrum of Li will be discussed. Finally, the theoretical results for Na nS and nD states are compared with our experiment [29].

All of the ionization mechanisms of Rydberg atoms exposed to BBR are illustrated in figure 1. The total BRR-induced ionization rate can be written as a sum of four separable contributions:

$$W_{BBR}^{tot} = W_{BBR} + W_{SFI} + W_{BBR}^{mix} + W_{SFI}^{mix}. \tag{2}$$

The first contribution, W_{BBR}, is the direct BBR photoionization rate of the initially excited nL state, which will be discussed in subsection 2.1. The second term, W_{SFI}, is the rate of SFI of high $n''L'$ Rydberg states, which are populated from the initial Rydberg state nL via absorption of BBR photons. This field ionization is discussed in subsection 2.3, while redistribution of population between Rydberg states is described in subsection 2.2. The third term, W_{BBR}^{mix}, is the total rate of BBR-induced photoionization of neighboring $n'L'$ Rydberg states, which are populated via spontaneous and BBR-induced transitions from the initial state. The last term, W_{SFI}^{mix}, is the rate of SFI of high-lying Rydberg $n''L'$ states that are populated in a two-step process via absorption of BBR photons by atoms in $n'L'$ states (note that here, in contrast to W_{SFI}, we consider lower $n'L'$, states which cannot be field ionized). The two latter ionization rates, which are related to population redistribution between Rydberg states, are considered in subsection 2.4. The atomic units will be used below, unless specified otherwise.

Experimental measurements of BBR-induced ionization rates are discussed in Section 3. The temperature dependence of BBR-induced ionization, measured by Spencer et al. [10], is discussed in subsection 3.1. The measured by us dependence of the BBR-induced ionization rates of Na Rydberg states on the principal quantum number n is presented in subsection 3.2. Application of the BBR-induced ionization to

the measurements of collisional ionization rates is discussed in subsection 3.3. The role of BBR in the formation of ultracold plasma is reviewed in subsection 3.4. Finally, the results of the present study are summarized in the Conclusion.

2. BBR-INDUCED IONIZATION: THEORETICAL APPROACH

2.1. Bound-bound transitions induced by blackbody radiation

We start the discussion of ionization of Rydberg atoms by BBR with the consideration of BBR-induced bound-bound transitions between Rydberg states, which have been studied most extensively. Blackbody radiation causes both transitions between Rydberg states and ac Stark shifts of energy levels [34–37]. Large dipole moments of Rydberg states make them sensitive to BBR. In addition, the spectral brightness of BBR at T=300 K (maximum at 2×10^{13} Hz) is relatively high for the low frequencies of transitions between Rydberg states.

Absorption of BBR by Rydberg atoms rapidly redistributes the initial population to neighboring states and thus reduces the selectivity of laser excitation. In contrast to the spontaneous decay of Rydberg atoms, which populates mostly ground and lower excited levels, the BBR-induced transitions populate predominantly the neighboring Rydberg states [see figure 1(b)]. Redistribution of the population of Rydberg states by BBR can be suppressed by surrounding the laser excitation volume with cooled shields. However, in order to reduce the rate of BBR-induced transitions by an order of magnitude, a liquid-helium cooling must be used.

Probabilities of BBR-induced transitions are proportional to the number of photons per mode of the blackbody radiation field [34]:

$$\bar{n}_\omega = \frac{1}{\exp\left(\omega/kT\right) - 1}, \tag{3}$$

where kT is the thermal energy in atomic units. For atoms in the ground and low excited states with large frequencies of transitions one has $\bar{n}_\omega \gg 1$ at T=300 K, and the rates of BBR-induced transitions are small. Hence, for atoms in those states interaction with BBR can be disregarded. The situation is different for Rydberg states: at transition frequencies on the order of 10 cm^{-1} we have $\bar{n}_\omega \sim 10$, and the rate of BBR-induced transitions can be ten times larger than the rate of the spontaneous decay to the neighboring Rydberg states.

Probability of a spontaneous transition between atomic nL and $n'L'$ levels is given by the Einstein coefficient $A\left(nL \to n'L'\right)$:

$$A\left(nL \to n'L'\right) = \frac{4\omega_{nn'}^3}{3c^3} \frac{L_{max}}{2L+1} R^2\left(nL \to n'L'\right). \tag{4}$$

Here, L_{max} is the largest of L and L', and $R\left(nL \to n'L'\right)$ is the radial matrix element of the electric dipole moment. The total rate of the spontaneous decay is a sum of rates

of transitions to all states with $n' < n$:

$$\Gamma_{nr} = \sum_{L'=L\pm1} \sum_{n'<E_n}^{n} A\left(nL \rightarrow n'L'\right). \tag{5}$$

The rate of BBR-induced transitions $W\left(nL \rightarrow n'L'\right)$ between the states nL and $n'L'$ is given by $A\left(nL \rightarrow n'L'\right)$ and the number of photons per mode of BBR at the transition frequency $\omega_{nn'} = 1/(2n^2) - 1/(2n'^2)$:

$$W\left(nL \rightarrow n'L'\right) = A\left(nL \rightarrow n'L'\right) \frac{1}{\exp\left(\omega_{nn'}/kT\right) - 1}. \tag{6}$$

In contrast to spontaneous decay, blackbody radiation populates states with the energy both higher and lower than that of the initially excited state. The total rate of BBR-induced transitions is a sum of rates of BBR-induced transitions to all $n'L'$ states:

$$\Gamma_{BBR} = \sum_{L'=L\pm1} \sum_{n'} \Gamma_{BBR}\left(n, L \rightarrow n', L'\right). \tag{7}$$

Blackbody radiation populates mostly the neighboring states with $n' = n \pm 1$, which give the main contribution to the total rate of BBR-induced transitions. This contribution to the total decay rate of the initially excited Rydberg state can be significant. The effective lifetime is inverse of the sum of total decay rates due to spontaneous and BBR-induced transitions:

$$\tau_{eff}^{-1} = \Gamma_{nr} + \Gamma_{BBR}. \tag{8}$$

The first experimental observation of depletion of Rydberg atoms due to BBR by Gallagher and Cooke [2] was based on measurements of the effective lifetimes of the $17P$ and $18P$ states of sodium.

A method to determine the effective lifetimes of Rydberg states was discussed by Gallagher in Ref. [34]. According to his calculations, the radiative lifetime of the sodium $18S$ state is 6.37 μs, but it reduces to 4.87 μs due to the interaction with BBR at T=300 K. This is consistent with time-resolved measurements of the fluorescence signal on the $18S \rightarrow 3P$ transition. The effective lifetime of the $18S$ state was also determined using the method of SFI [30], which is the only reliable way to measure the population of a Rydberg state. Any Rydberg atom ionizes with a probability close to unity if the electric-field strength has reached a critical value E_c (see figure 2). The latter strongly depends on the effective quantum number $n_{eff} = n - \mu_L$, where μ_L is the quantum defect:

$$E_c \approx 3.2 \cdot 10^8 n_{eff}^{-4} \quad \left(\mathrm{V/cm}\right). \tag{9}$$

Unfortunately, SFI is difficult to use for Rydberg states with low n, since it requires very strong electric fields ($\sim$30 kV/cm for $n \sim$10).

Haroche et al. [38] observed that the decay of the $25S$ state of Na is accompanied by population of the neighboring states including the $25P$ state, which could be populated only due to BBR. Later, in a well-known paper [8] Theodosiou published the calculated

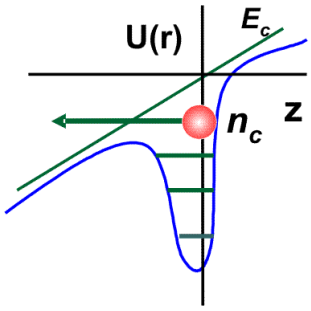

Figure 2. Illustration of the selective field ionization (SFI) of a Rydberg atom with a principal quantum number n_c by electric field with the amplitude E_c.

effective lifetimes of nS, nP, nD, and nF Rydberg states of alkali-metal atoms with $n < 20$ at the ambient temperatures of 0, 350, 410, and 600 K. These values were obtained using the accurate and reliable method of model potential.

Redistribution of population of Xe Rydberg states by BBR was studied by Beiting et al. [39] using the SFI method. The results of numeric calculations of depopulation rates of nS, nP and nD ($n < 30$) Rydberg states induced by BBR were published in [9]. Radial matrix elements of electric dipole transitions for states with $n < 15$ were calculated using the Bates-Damgaard method. For higher Rydberg states the calculations were done in the Coulomb approximation using the Numerov method [40]. The populations of neighboring Rydberg states were calculated using a one-step model, which took into account only the direct transitions from the initially excited state. Suppose a chosen nS state is initially excited. The time-dependent number of Rydberg atoms in this state is determined by its effective lifetime τ_{eff}^{nS}:

$$N_{nS}(t) = N_{nS}(0) \exp\left(-t/\tau_{eff}^{nS}\right), \tag{10}$$

where $N_{nS}(0)$ is the number of Rydberg atoms in the nS state at time t=0. The number of atoms in the neighboring $n'P$ states is determined by two competing processes: (i) transitions [spontaneous at the rate $A(nS \to n'P)$ and BBR-induced at the rate $W(nS \to n'P)$ $\sim 10^4$ s^{-1}] from nS states with $n \sim 15$, and (ii) spontaneous decay of $n'P$ states with $n' \sim 15$ at the rate $\Gamma_{eff}^{n'P} (\sim 10^5\,\mathrm{s}^{-1})$:

$$\frac{dN_{n'P}(t)}{dt} = \left[W(nS \to n'P) + A(nS \to n'P)\right] N_{nS}(t) - \Gamma_{eff}^{n'P} N_{n'P}(t). \tag{11}$$

The $n'P$ states are not populated initially. A solution of equations (10) and (11) with the initial condition $N_{n'P}(0) = 0$ is:

$$N_{n'P}(t) = \frac{\left[W(nS \to n'P) + A(nS \to n'P)\right] N_{nS}(0)}{\Gamma_{eff}^{n'P} - \Gamma_{eff}^{nS}} \times \times \left(\exp\left(-\Gamma_{eff}^{nS} t\right) - \exp\left(-\Gamma_{eff}^{n'P} t\right)\right). \tag{12}$$

The range of applicability of the one-step model was discussed by Galvez et al. [14]. They have developed a multistep model and studied the redistribution of population theoretically and experimentally. Rydberg atoms in a sodium atomic beam were excited by two pulsed dye lasers. The number density of ground-state atoms in the interaction region was varied from 8×10^9 cm^{-3} to 2×10^{10} cm^{-3}. At the time t_d after the excitation, the populations of Rydberg states were detected using the time-resolved SFI method [30] by an electric filed pulse with the amplitude of 1 kV and the duration of 4 μs, which was sufficient to ionize all states with $n \geq 24$. When the delay time t_d was increased from 0 to 40 μs, additional peaks in the field ionization spectrum appeared, indicating that neighboring Rydberg states were populated by BBR.

The population N_i of the ith Rydberg state is a solution of a system of differential equations [14]:

$$\frac{dN_i}{dt} = -N_i \sum_j \Gamma^i_j + \sum_k N_k \Gamma^k_i, \tag{13}$$

which take into account the multistep transitions. Here, Γ^i_j is the total rate of transitions between states i and j. The first term in the rhs of equation (13) describes the decay of state i, while second term gives the population of state i due to the decay from higher states populated by BBR. The authors of Ref. [14] solved a system of 32 equations (13) for $(n+1)S$, nP, nD and nF states with n=25-32. One-, two- and three-step transitions were taken into account, while for higher steps it was necessary to take into account the states with larger orbital momenta. However, it was shown that the population of nF states was small, and the contribution from states with larger L can be neglected. Evolution of Rydberg state populations was calculated numerically. Radial matrix elements were calculated using the Van Regermorter method [41], which is fast and agrees with the more complicated Numerov method at an accuracy level of 1%. The results showed that if the delay time t_d is comparable with the lifetime of the initially excited state, the multi-step transitions play an important role in the population redistribution, which cannot be described using the one-step model. BBR-induced resonances between Stark states of sodium Rydberg atoms have also been studied [15].

The above consideration of BBR-induced transitions between Rydberg states was based on the electric dipole approximation and perturbation theory. The range of applicability of such approach was analyzed by Farley and Wing [9]. At the room temperature T=300 K, the energy of BBR photons is comparable with the energy of Coulomb interaction of Rydberg electron with the atomic core at $n \sim 120$, which is the limit of applicability for the perturbation theory. The dipole approximation breaks down when the wavelength of BBR is comparable with the orbit size of the Rydberg electron ($n \sim 200$ at the room temperature).

2.2. Direct BBR photoionization

The direct BBR photoionization rate W_{BBR} of a given nL state is calculated from the general formula [10]:

$$W_{BBR} = c \int_{\omega_{nL}}^{\infty} \sigma_\omega \, \rho_\omega d\omega, \tag{14}$$

where c is the speed of light, $\omega_{nL} = 1/\left(2n_{eff}^2\right)$ is the photoionization threshold frequency for nL Rydberg state with the effective principal quantum number n_{eff}, and σ_ω is the photoionization cross-section at frequency ω. The volume density ρ_ω of BBR photons at temperature T is given by the Plank distribution:

$$\rho_\omega = \frac{\omega^2}{\pi^2 c^3 \left[\exp\left(\omega/kT\right) - 1\right]}. \tag{15}$$

For isotropic and non-polarized thermal radiation field the value of σ_ω is determined by the radial matrix elements $R\left(nL \to E, L \pm 1\right)$ of dipole transitions from discrete nL Rydberg states to the continuum states with $L\pm1$ and photoelectron energy E:

$$\sigma_\omega = \frac{4\pi^2 \omega}{3c\left(2L+1\right)} \sum_{L'=L\pm1} L_{max} R^2\left(nL \to E, L \pm 1\right), \tag{16}$$

where L_{max} is the largest of L and L'.

The main problem in the calculation of W_{BBR} for an arbitrary Rydberg state is associated with finding $R\left(nL \to E, L \pm 1\right)$ and its frequency dependence. In order to achieve a high accuracy of the matrix elements, numerical calculations should be used.

Spencer et al. [10] studied the temperature dependence of the rate of direct BBR-induced photoionization W_{BBR} of the $17D$ state of Na. The values of W_{BBR} were calculated numerically and a simple formula was obtained:

$$W_{BBR} \sim E_n^2 \left[\exp\left(\frac{E_n}{kT}\right) - 1\right]^{-1}, \tag{17}$$

where E_n is the energy of the Rydberg electron. This approximate formula was used for estimates of W_{BBR} in many recent works on ultracold plasma [16, 19]. Accurate numerical calculations of W_{BBR} using the method of model potential were done by Lehman [11] for principal quantum numbers n=10-40 and temperatures T=77-625 K, but only for sodium and hydrogen atoms. Recently, the method of model potential was used by Glukhov and Ovsiannikov [42] to calculate W_{BBR} of helium nS, nP and nD Rydberg states. A simple analytical formula which approximates the numerical results was obtained:

$$W_{BBR} = \left(a_1 x^2 + a_2 x^3 + a_3 x^4\right) \frac{1}{\exp\left(x\right) - 1}, \quad x = \frac{E_n}{kT}. \tag{18}$$

The coefficients a_1, a_2, a_3 depend on the ambient temperature T:

$$a_i = \sum_{k=0}^{3} b_{ik} \left(\frac{T}{100}\right)^k. \tag{19}$$

The coefficients b_{ik}, which depend only on L, were calculated independently for singlet and triplet S, P and D states of helium.

In present study we used the semi-classical formulas for dipole matrix elements derived by Dyachkov and Pankratov [43, 44]. In comparison with other semi-classical methods [45,46], these formulas are advantageous as they give orthogonal and normalized continuum wave functions, which allow for the calculation of photoionization cross-sections with high accuracy. We have verified that photoionization cross-sections of the lower sodium S states calculated using the approach of [44] are in good agreement with the sophisticated quantum-mechanical calculations by Aymar [47].

A more accurate analytical expression for W_{BBR} than equation (17) is useful in order to illustrate the dependence of ionization rate on n, L, and T. We have obtained such expression using the analytical formulas for bound-bound and bound-free matrix elements derived by Goreslavsky, Delone, and Krainov (GDK) [45] in the quasiclassical approximation. For the direct BBR photoionization of a nL Rydberg state the cross-section is given by:

$$\sigma_\omega\left(nL \to E, L \pm 1\right) = \frac{4L^4}{9cn^3\omega}\left[K_{2/3}^2\left(\frac{\omega L^3}{3}\right) + K_{1/3}^2\left(\frac{\omega L^3}{3}\right)\right], \tag{20}$$

where $K_\nu\left(x\right)$ is the modified Bessel function of the second kind. This formula was initially derived to describe the photoionization of hydrogen atoms.

The main contribution to W_{BBR} in equation (14) comes from ionization by BBR of frequencies close to the ionization threshold frequency ω_{nL}, because the Plank distribution rapidly decreases with increasing ω. For Rydberg states with $n>>1$ and low L one has $(\omega L^3/3) << 1$, and equation (20) can be simplified to the form:

$$\sigma_\omega\left(nL \to E, L \pm 1\right) \approx \frac{1}{9cn^3}\left[\frac{6^{4/3}\Gamma^2\left(2/3\right)}{\omega^{7/3}} + \frac{6^{2/3}\Gamma^2\left(1/3\right)}{\omega^{5/3}}L^2\right]. \tag{21}$$

The combination of equations (14), (18) and (20) yields:

$$W_{BBR} \approx \frac{1}{\pi^2 c^3 n^3}\int\limits_{\omega_{nL}}^{\infty}\left[2.22\,\omega^{-1/3} + 2.63\,\omega^{1/3}L^2\right]\frac{d\omega}{\exp\left(\omega/kT\right) - 1}. \tag{22}$$

The expression in the square brackets is a slowly varying function of ω. Taking into account that the main contribution to W_{BBR} is due to frequencies close to the ionization threshold frequency, one can replace in the square brackets ω by $1/(2n^2)$. After such replacement the integral in equation (22) can be calculated analytically, and the final result is:

$$W_{BBR} \approx \frac{kT}{\pi^2 c^3}\left[\frac{2.80}{n^{7/3}} + \frac{2.09L^2}{n^{11/3}}\right]\ \ln\left(\frac{1}{1 - \exp\left(-\frac{\omega_{nL}}{kT}\right)}\right). \tag{23}$$

Equation (23) gives the approximate direct BBR-induced photoionization rate in atomic units for T measured in Kelvins.

In Ref. [45] it was proposed that equation (20) can be extended to alkali-metal atoms simply by replacing n with $n_{eff} = (n - \mu_L)$. In the reality, however, its accuracy is acceptable only for truly hydrogen-like states with small quantum defects. A disadvantage of the GDK model is that it disregards the non-hydrogenic phase factors in the overlap integrals of dipole matrix elements. Nevertheless, we suggest that for alkali-metal atoms equation (23) can be rewritten as follows (for convenience W_{BBR} is expressed in s^{-1} for temperature T taken in Kelvins):

$$W_{BBR} = C_L T \left[\frac{14423}{n_{eff}^{7/3}} + \frac{10770 L^2}{n_{eff}^{11/3}} \right] \ln \left(\frac{1}{1 - \exp\left(-\frac{157890}{T n_{eff}^2} \right)} \right) \quad \left[s^{-1} \right]. \quad (24)$$

Here, C_L is an L-dependent scaling coefficient, which will be discussed below. A comparison of the numerically calculated W_{BBR} with equation (24) at C_L=1 has shown a noticeable disagreement of absolute values of W_{BBR}, especially for nS states, which have large quantum defects (for example, in sodium atoms the quantum defects are μ_S=1.348, μ_P=0.855 and μ_D=0.015). Formally, the disagreement for the non-hydrogenic nS states stems from peculiarities of the asymptotic behavior of Bessel functions in equation (20) for states with $L \ll 1$. For example, the analytical expression of GDK model yields close photoionization cross-section values for the sodium nS, nP and nD states, while the accurate numerical calculations yield significantly smaller cross-sections for the sodium nS states. At the same time, the shapes of the analytical curves are quite similar to the numerical ones. Therefore, it is reasonable to introduce a scaling coefficient C_L in equation (24) in order to make it valid for Rydberg states of alkali-metal atoms with large quantum defects.

In fact, the scaling coefficient C_L accounts for phase shifts of radial wave functions of alkali-metal Rydberg states due to quantum defect. Delone, Goreslavsky and Krainov [48] suggested an approximate formula to calculate the radial matrix elements of transitions between continuum states of non-hydrogen atoms:

$$R_{EL}^{El'} \approx \frac{0.4744}{\omega^{5/3}} \cos\left(\Delta_L \pm \frac{\pi}{6} \right). \quad (25)$$

Here, $\Delta_L = |\pi (\mu_{L'} - \mu_L)|$ is the difference of quantum defects of L and L' states, the $(+)$ sign corresponds to transitions with $L' > L$ and the $(-)$ sign corresponds to transitions with $L' < L$. In order to take into account the phase shifts of non-hydrogen wave functions, we have empirically introduced the corrected non-hydrogen radial matrix elements:

$$\tilde{R}_{nL}^{EL+1} \sim R_{nL}^{EL+1} \cos\left(\Delta_L^+ + \frac{\pi}{6} \right), \quad \tilde{R}_{nL}^{EL-1} \sim R_{nL}^{EL-1} \cos\left(\Delta_L^- - \frac{\pi}{6} \right). \quad (26)$$

Here, $\Delta_L^+ = \pi (\mu_L - \mu_{L+1})$, $\Delta_L^- = \pi (\mu_{L-1} - \mu_L)$, and $R_{nL}^{EL\pm1}$ are radial matrix elements of bound-free transitions calculated in the hydrogen GDK model with n replaced by n_{eff}. The differences of quantum defects $\mu_L - \mu_{L'}$ [49–56] for transitions from Rydberg states with $n \sim 20$ to continuum are summarized in Table 1 for all alkali-metal atoms.

Table 1. Difference of quantum defects of alkali-metal Rydberg states.			
	$\mu_S - \mu_P$	$\mu_P - \mu_D$	$\mu_D - \mu_F$
Li	0.352417	0.0451664	0.00162407
Na	0.493519	0.840023	0.0148029
K	0.466733	1.43762	0.264237
Rb	0.490134	1.29456	1.34636
Cs	0.458701	1.12661	2.43295

In the calculations of photoionization rates for low-L states, the terms of equation (20) proportional to L and L^2 can be neglected. Taking into account equation (25), equation (24) can be rescaled in order to achieve a better agreement with the numerical results:

$$W_{BBR} = A_L \frac{11500T}{n_{eff}^{7/3}} \left[\cos\left(\Delta_L^+ + \frac{\pi}{6}\right)^2 + \cos\left(\Delta_L^- - \frac{\pi}{6}\right)^2\right] \times \tag{27}$$
$$\times \ln\left[\frac{1}{1-\exp\left(-\frac{157890}{Tn_{eff}^2}\right)}\right] \quad \left[\mathrm{s}^{-1}\right].$$

Here, $A_L \sim 1$ is the new scaling coefficient, which is only slightly different for nS, nP and nD Rydberg states of various alkali-metal atoms, in contrast to C_L that ranges from 0.003 for lithium nS states to 1 for sodium nD states. For nS states, only the first term in the square brackets of equation (27) corresponding to transitions with $L' = L + 1$ must be considered.

For estimates of the direct BBR photoionization rates with the accuracy or 50% it is sufficient to choose $A_L = 1$. For more accurate calculations the values of A_L can be taken from Table 2. We have obtained these values by comparing the results of analytical and more accurate numerical calculations. The coefficients are close to unity, except nP states of potassium and nD states of rubidium and cesium.

Table 2. Numerically determined scaling coefficients A_L in equation (27).			
	A_S	A_P	A_D
Li	1	1	0.9
Na	1	1	1.1
K	0.9	0.45	1.3
Rb	1	1	0.6
Cs	0.85	1.1	0.35

The results of our numerical and analytical calculations of the direct BBR photoionization rates of alkali-metal Rydberg atoms are presented in figure 3. Figure 3(a) shows the dependence of W_{BBR} on the quantum defect for the $30S$ Rydberg state of different alkali-metal atoms at the temperature T=300 K. A good agreement between the numerical results and formula (27) with A_L=1 is found. For nP and nD states such a simple dependence cannot be obtained because, in contrast to nS states, there are two ionization channels with $L' = L+1$ and $L' = L-1$ involved. Figures 3(b)-(d) present the results for nS, nP and nD states of lithium with n=5-80 at three ambient temperatures T=77, 300, and 600 K (coefficients A_L are taken from Table 2). For nP and nD states [figures 3(c) and (d)] the formula (27) agrees well with the numerical results, while for nS states [figure 3(b)] the shapes of numerical and analytical curves are completely different. This is caused by strongly non-hydrogenic character of lithium nS states, which will be discussed in detail in Section 2.3.

Results of calculations of W_{BBR} for Na, K, Rb, and Cs atoms in nS, nP, and nD Rydberg states with n=5-80 at the ambient temperatures of T=77, 300, and 600 K are presented in figures 4 and 5. In addition, our numerical and analytical calculations for Na are compared with the results by Lehman [11] and a good agreement is observed [see figure 4(a),(b),(c)]. For other alkali-metal Rydberg states such a comparison is not possible because, to the best of our knowledge, no other published data are available.

A good agreement between the numerical and analytical results is found for $n < 50$. For higher n the accuracy of the analytical formula decreases and becomes worse than 50% at $n\sim$100 for nP states. For higher L, a neglected contribution from the terms proportional to L and L^2 in equation (27) becomes more important. However, keeping these terms in equation (27) complicates the formula but does not substantially improve the accuracy.

We note that analytical formula (27) uses an asymptotic expansion of the MacDonald functions, which is valid at $\omega L^3 << 1$. In the slow-varying part of the integral (22) in the square brackets we replaced ω by $1/2n_{eff}^2$. Such replacement formally requires $\omega_{nL} > kT$ (at temperature T=300 K it is correct only for states with $n < 20$). Nevertheless, a comparison with our numerical results has shown that equation (27) actually gives correct estimates of BBR ionization rates also for higher values of n (up to $n\sim$50). We conclude that equation (27) is applicable for $L << n$ and provides accurate estimates of BBR-induced photoionization rates of nS, nP and nD alkali-metal Rydberg states.

2.3. BBR-induced mixing of Rydberg states

BBR causes not only direct photoionization of the initially populated Rydberg levels. It also induces transitions between neighboring Rydberg states, thus leading to population redistribution [14, 15, 57]. For example, after laser excitation of the Na $16S$ state, the BBR-induced transitions populate the neighboring $n'P$ states [figure 1(a)]. The calculations show that these states have significantly higher direct photoionization rates

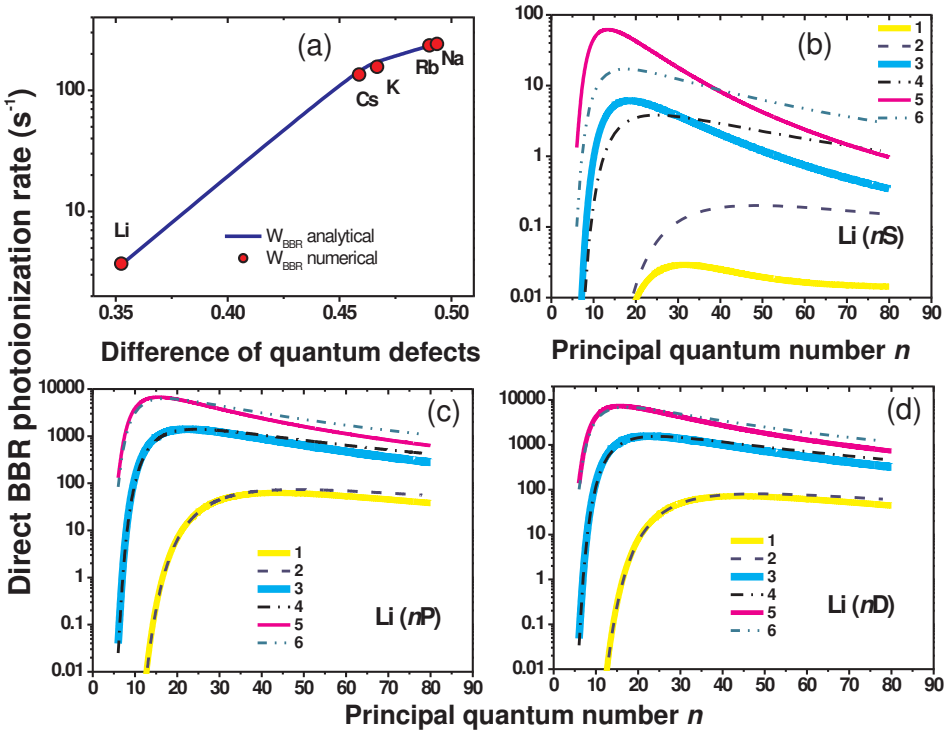

Figure 3. Direct BBR photoionization rates of alkali-metal Rydberg states. (a) Dependence of the photoionization rates of the $30S$ state of lithium, sodium, potassium, rubidium, and cesium at T=300 K on the difference of quantum defects $\mu_S - \mu_P$; (b), (c), (d) - dependence of the photoionization rates of lithium nS, nP, and nD Rydberg states on the principal quantum number n. Curves (1), (3), (5) are numerical results obtained using the Dyachkov and Pankratov model at the ambient temperatures T=77, 300, and 600 K, respectively. Curves (2), (4), (6) are analytical results obtained using equation (27) at the ambient temperatures T=77, 300, and 600 K, respectively.

than the $16S$ state itself. Hence, BBR-induced population transfer to $n'P$ states can noticeably affect the effective BBR photoionization rate. The rates of spontaneous and BBR-induced transitions from the initial $16S$ and $16D$ states to $n'P$ states have been calculated by us in [29] and are shown in figures 1(b) and (c).

Importantly, absorption of BBR induces also transitions to higher Rydberg states, which are denoted as n'' in figure 1(a). These states can be ionized by the electric field pulses usually applied in experiments in order to extract ions into ionization detectors.

2.4. Field ionization of high Rydberg states populated by BBR

Extraction electric-field pulses, which are commonly used to extract ions from the ionization zone to the ionization detector, ionize all Rydberg states with effective quantum numbers n_{eff} exceeding some critical value n_c. This critical value n_c depends on the amplitude of the applied electric field and it can be found from the approximate

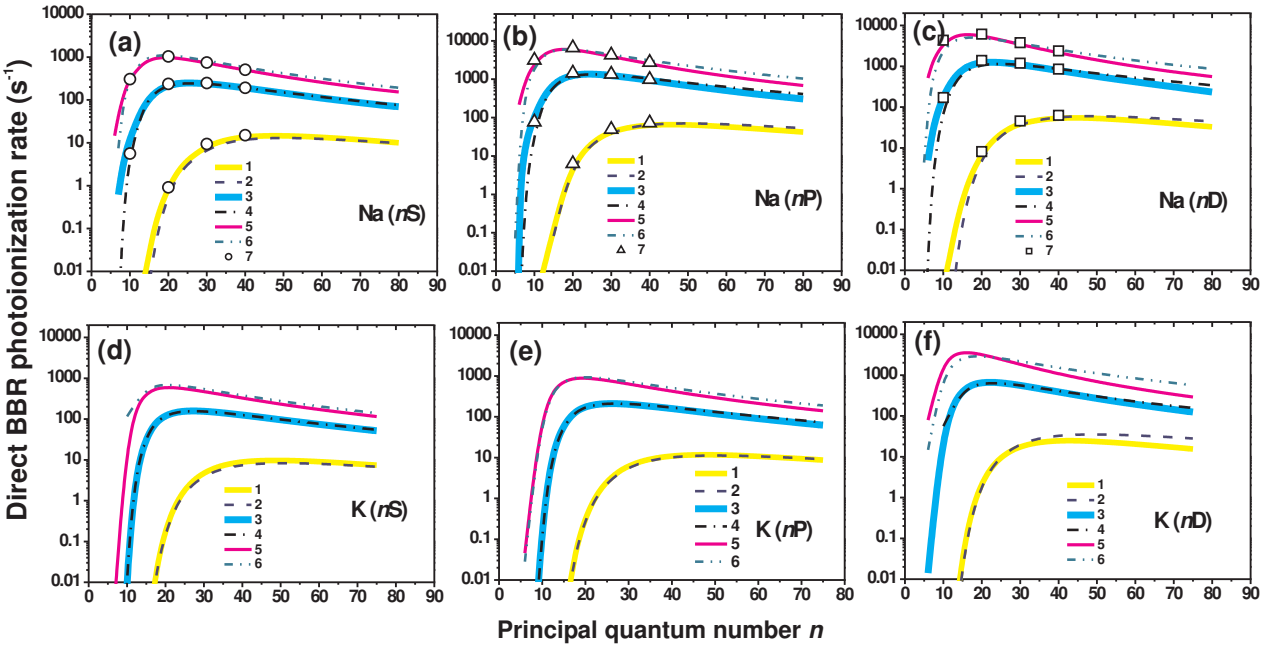

Figure 4. Direct BBR photoionization rates of (a) nS, (b) nP, and (c) nD Rydberg states of sodium, and (d) nS, (e) nP, and (f) nD Rydberg states of potassium. Curves (1), (3), (5) are numerical results obtained using the Dyachkov and Pankratov model at the ambient temperatures T=77, 300, and 600 K, respectively. Curves (2), (4), (6) are analytical results obtained using equation (27) at the ambient temperatures T=77, 300, and 600 K, respectively. Curve (7) shows the numerical results for sodium published by Lehman [11].

formula (9). Hence, if a BBR mediated process populates a state with $n' \geq n_c$, this state will be ionized and thus will contribute to the detected ionization signal [10].

In order to analyze the efficiency of this process, we calculated the radial matrix elements $R(nL \rightarrow n'L')$ of dipole-allowed transitions to other $n'L'$ states with $L' = (L \pm 1)$ using the semi-classical formulas of [44]. The total rate W_{SFI} of BBR transitions to all Rydberg states with $n' \geq n_c$ can be calculated by summing the individual contributions of $nL \rightarrow n'L'$ transitions given by equation (6):

$$W_{SFI} = \sum_{n' \geq n_c} \sum_{L'=L\pm 1} W(nL \rightarrow n'L'). \tag{28}$$

We have numerically calculated the values of W_{SFI} for various amplitudes E of the electric-field pulses.

We also compared the numerical values with those obtained from the approximate analytical formulae, which have been derived using the bound-bound matrix elements of the GDK model:

$$W_{SFI} \approx \frac{1}{\pi^2 c^3 n^3} \int_{\frac{1}{2n^2}-\frac{1}{2n_c^2}}^{\omega_{nL}} \left[2.22\,\omega^{-1/3} + 2.63\,\omega^{1/3}L^2\right] \frac{d\omega}{\exp(\omega/kT) - 1}. \tag{29}$$

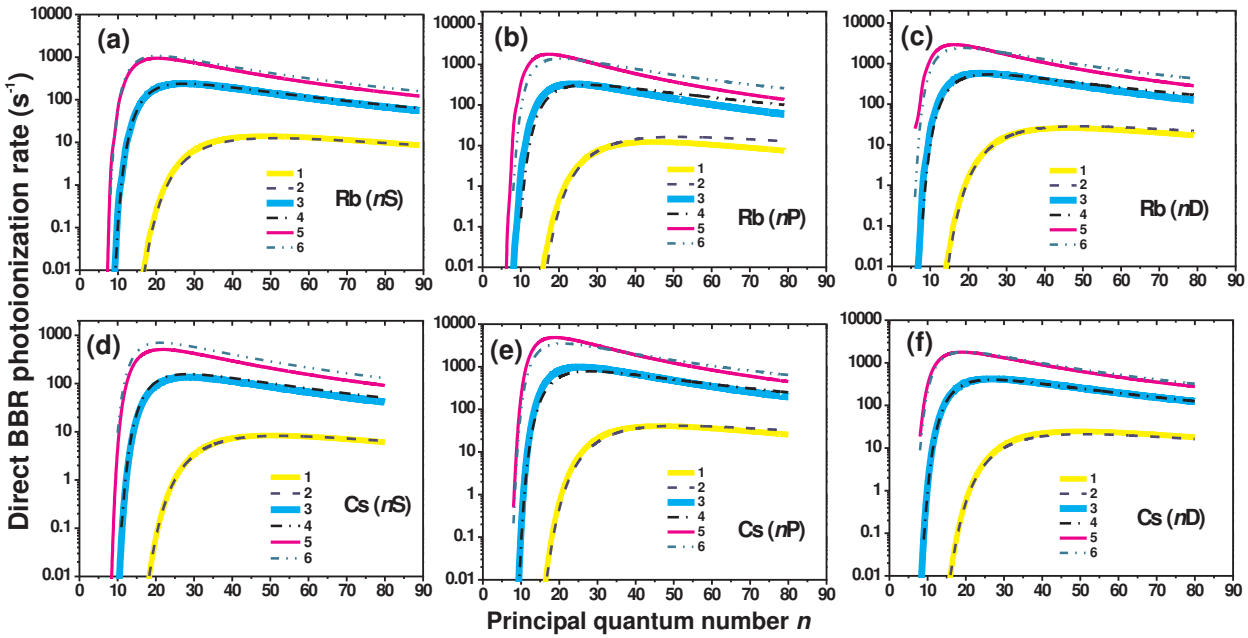

Figure 5. Direct BBR photoionization rates of (a) nS, (b) nP, and (c) nD Rydberg states of rubidium, and (d) nS, (e) nP, and (f) nD Rydberg states of cesium. Curves (1), (3), (5) are numerical results obtained using the Dyachkov and Pankratov model at the ambient temperatures T=77, 300, and 600 K, respectively. Curves (2), (4), (6) are analytical results obtained using equation (27) at the ambient temperatures T=77, 300, and 600 K, respectively.

The integration limits are chosen such that the integral accounts for transitions to those Rydberg states for which $\left(\frac{1}{2n^2}-\frac{1}{2n_c^2}\right)<\omega<\omega_{nL}$ (i.e., states above the field ionization threshold). Integration of equation (29) in the same approximation as for equation (22) gives another useful analytical formula that is similar to equation (27):

$$W_{SFI}=A_L\frac{11500T}{n^{7/3}}\left[\cos\left(\Delta_L^{+}+\tfrac{\pi}{6}\right)^2+\cos\left(\Delta_L^{-}-\tfrac{\pi}{6}\right)^2\right]\times$$
$$\times\left[\ln\frac{1}{1-\exp\left(\frac{157890}{Tn_c^2}-\frac{157890}{Tn^2}\right)}-\ln\frac{1}{1-\exp\left(-\frac{157890}{Tn^2}\right)}\right]\quad \mathrm{s}^{-1}\quad , \tag{30}$$

where T is in Kelvins.

The obtained numerical and analytical data on W_{SFI} calculated for nS, nP, and nD alkali-metal Rydberg states with n=5-80 at the ambient temperatures T=77, 300, and 600 K and the amplitudes of the electric field of 5 and 10 V/cm are presented in figures 6-8. The scaling coefficients A_L from Table 2 have been used.

We have unexpectedly found that the dependence of W_{SFI} on n for lithium nS Rydberg states exhibits a deep minimum at $n\sim$30 [figure 6(a)]. For nP and nD states of lithium and nS, nP and nD states of other alkali-metal Rydberg atoms such a minimum is absent [figures 7-8]. A theoretical analysis has shown that this anomaly is caused by a

Cooper minimum in the discrete spectrum for transitions between nS and $n'P$ lithium Rydberg states [58]. It can be explained as follows. For hydrogen atoms the radial matrix elements of transitions between bound Rydberg states decrease monotonously with increase of the interval between energy levels. In contrast, the radial wave functions of alkali-metal Rydberg states have varying phase shifts $\pi\mu_l$, which can suppress the overlapping between wave functions in the calculated radial matrix elements of the electric dipole moment [59]. This leads to a minimum in transition probabilities, which are proportional to the square of radial matrix elements. The hydrogenic GDK model [dashed curve in figure 6(a)] does not predict a Cooper minimum, since the phase shifts of radial wave functions due to quantum defects are ignored.

For hydrogen-like nP and nD lithium Rydberg states [figure 6(b) and (c), respectively] the analytical and numerical calculations give close results, although the agreement between them is worse than in the case of the direct photoionization by BBR. The same is observed for nS, nP and nD Rydberg states of sodium, potassium, rubidium, and cesium [figures 7-8].

The chosen amplitudes of the electric field of 5 and 10 V/cm correspond to the typical conditions of experiments with laser-cooled Rydberg atoms, because such fields do not lead to ionization of Rydberg states with large quantum numbers n ∼30-50 relevant to experiments on ultracold plasma [19]. Such electric fields are just sufficient to extract from the interaction volume ions formed due to collisional and BBR-induced ionization of Rydberg atoms. At n ∼30 the rate of ionization by electric field is by an order of magnitude smaller than the rate of direct BBR-induced photoionization. The rates of direct BBR photoionization and BBR-induced SFI become comparable at n∼60.

In our experiment (subection 3.1) we used sodium Rydberg atoms in states with low n ∼8-20, which were interesting in the context of collisional ionization studies. The experimental conditions required the use of extracting electric pulses of larger amplitude (100 V/cm). The results of the calculation of W_{SFI} for nS and nD sodium Rydberg atoms by the 100 V/cm and 200 V/cm electric pulses are shown in figure 9. The calculations were made only for n=5-35, since Rydberg states with $n > 37$ are ionized by the 200 V/cm electric field. For n ∼20 the rate of direct BBR photoionization is only two times larger than W_{SFI}. Hence, the contribution of BBR-induced SFI is important.

2.5. Total BBR-induced ionization rates

In this section we shall analyze the time evolution of populations of Rydberg states during the interaction with ambient BBR photons. A typical timing diagram for the laser excitation of Rydberg states and detection of ions created by SFI is shown in figure 10. This scheme was used in our recent experiment on collisional ionization of Na Rydberg atoms [29]. The electric field was formed by two metallic plates, one of them having a hole with a mesh allowing the extraction of ions. Two identical electric field pulses with the 100 V/cm amplitude and 250 ns duration [figure 10(b)] were applied to

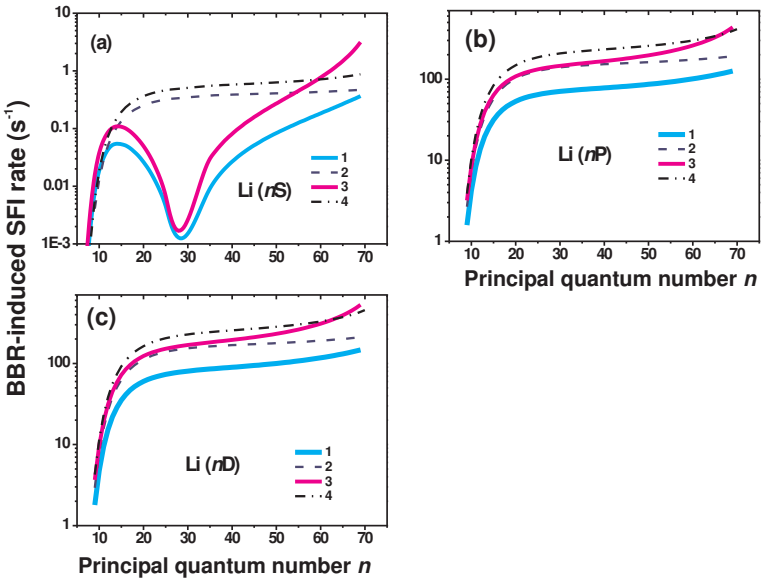

Figure 6. Calculated BBR-induced SFI rates W_{SFI} for (a) nS, (b) nP, and (c) nD Rydberg states of lithium at the ambient temperature of 300 K. Curves (1) and (3) are numerical results obtained using the Dyachkov and Pankratov model at the electric-field amplitudes of E=5 and 10 V/cm, respectively. Curves (2) and (4) are analytical results obtained using equation (30) at the electric-field amplitudes of E=5 and 10 V/cm, respectively.

the repelling plate after each laser excitation pulse [figure 10(a)]. The first pulse was applied immediately after the laser pulse to remove the atomic A^+ and the molecular A_2^+ ions produced during the laser pulse. The second pulse extracted to a particle detector (channeltron) those ions, which appeared in the time interval between $t_1 = 0.3\,\mu$s and $t_2 = 2.1\,\mu$s after the laser excitation pulse. These ions appeared due to collisional and BBR-induced ionization of Rydberg atoms. In the mass spectrum detected by the channeltron, the signals of the atomic A^+ and the molecular A_2^+ ions were separated by 0.6 μs and thus well resolved [figure 10(c)]. The gated pulse counters registered the signals from the atomic and molecular ions independently [figure 10(d)].

Let us first consider the simplest case of laser excitation of a single sodium nS state. The evolution of the number N_{A^+} of atomic ions produced via absorption of BBR photons by atoms in the initial nS state is given by

$$\frac{dN_{A^+}(t)}{dt} = W_{BBR} N_{nS}(t)\,, \tag{31}$$

where $N_{nS}(t) = N_{nS}(t=0)\exp\left(-t/\tau_{eff}^{nS}\right)$ is the total number of Rydberg atoms remaining in the nS state as a function of time, and τ_{eff}^{nS} is the effective lifetime of the nS state. The number of photoions produced by BBR during the time interval (t_1, t_2) is of interest. The total number of ions produced during this interval by direct BBR photoionization of the nS state can be found by integrating equation (31) from t_1

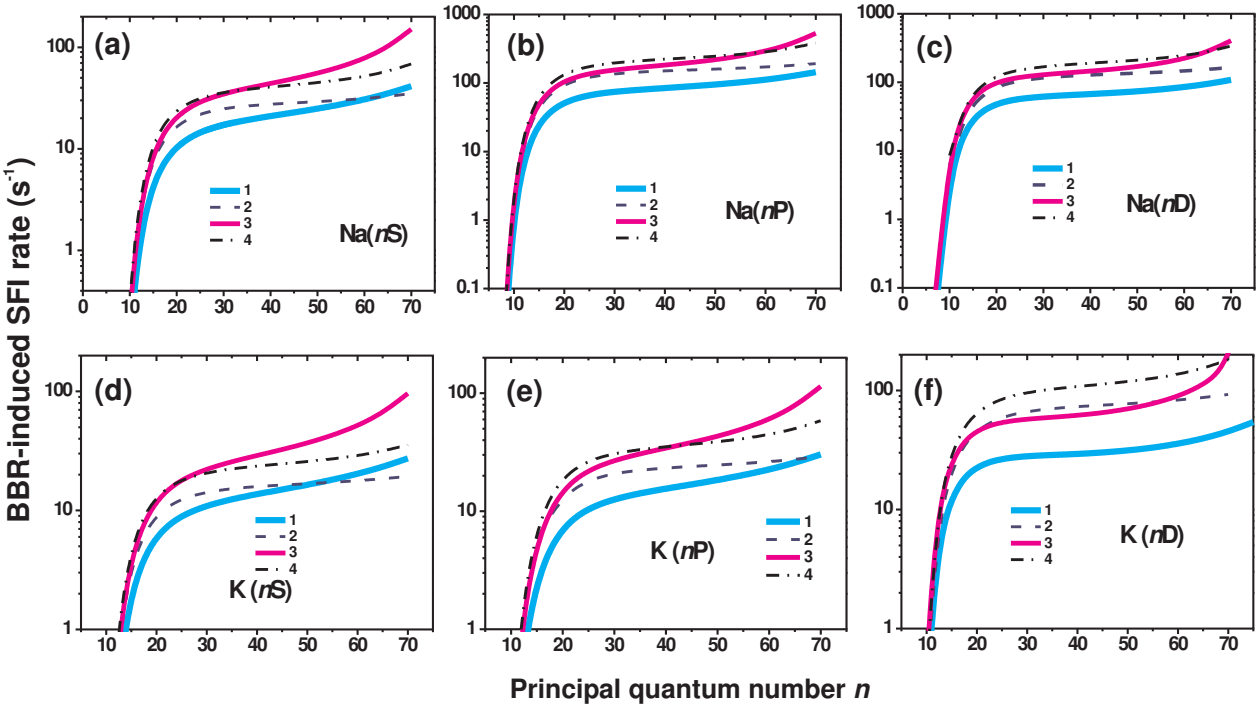

Figure 7. Calculated BBR-induced SFI rates W_{SFI} for (a) nS, (b) nP, and (c) nD Rydberg states of sodium, and (d) nS, (e) nP, and (f) nD Rydberg states of potassium at the ambient temperature of 300 K. Curves (1) and (3) are numerical results obtained using the Dyachkov and Pankratov model at the electric-field amplitudes of E=5 and 10 V/cm, respectively. Curves (2) and (4) are analytical results obtained using equation (30) at the electric-field amplitudes of E=5 and 10 V/cm, respectively.

to t_2:

$$N_{A^+} = N_{nS}\left(t=0\right) W_{BBR} \tau_{eff}^{nS} \left[\exp\left(-t_1/\tau_{eff}^{nS}\right) - \exp\left(-t_2/\tau_{eff}^{nS}\right)\right]. \qquad (32)$$

This result can be rewritten by introducing an effective interaction time t_{eff}^{nS} [29]:

$$\begin{aligned} N_{A^+} &= N_{nS}\left(t=0\right) W_{BBR} t_{eff}^{nS}, \qquad (33)\\ t_{eff}^{nS} &= \tau_{eff}^{nS} \left[\exp\left(-t_1/\tau_{eff}^{nS}\right) - \exp\left(-t_2/\tau_{eff}^{nS}\right)\right]. \end{aligned}$$

Blackbody radiation induces also transitions to other Rydberg states $n'P$, as discussed in section 2.2. Evolution of populations of these states is described by the rate equation

$$\begin{aligned} \frac{dN_{n'P}\left(t\right)}{dt} &= \left[W\left(nS \rightarrow n'P\right) + A\left(nS \rightarrow n'P\right)\right] N_{nS}\left(t\right) - \qquad (34)\\ &\quad - N_{n'P}\left(t\right) \Big/ \tau_{eff}^{n'P}, \end{aligned}$$

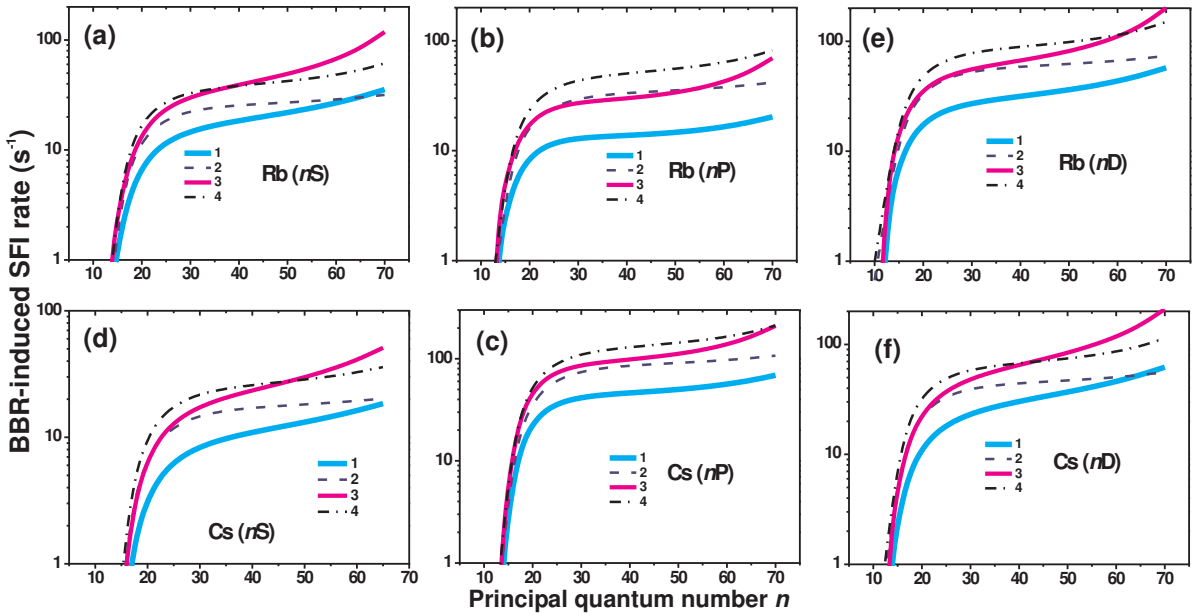

Figure 8. Calculated BBR-induced SFI rates W_{SFI} for (a) nS, (b) nP, and (c) nD Rydberg states of rubidium, and (d) nS, (e) nP, and (f) nD Rydberg states of caesium at the ambient temperature of 300 K. Curves (1) and (3) are numerical results obtained using the Dyachkov and Pankratov model at the electric-field amplitudes of E=5 and 10 V/cm, respectively. Curves (2) and (4) are analytical results obtained using equation (30) at the electric-field amplitudes of E=5 and 10 V/cm, respectively.

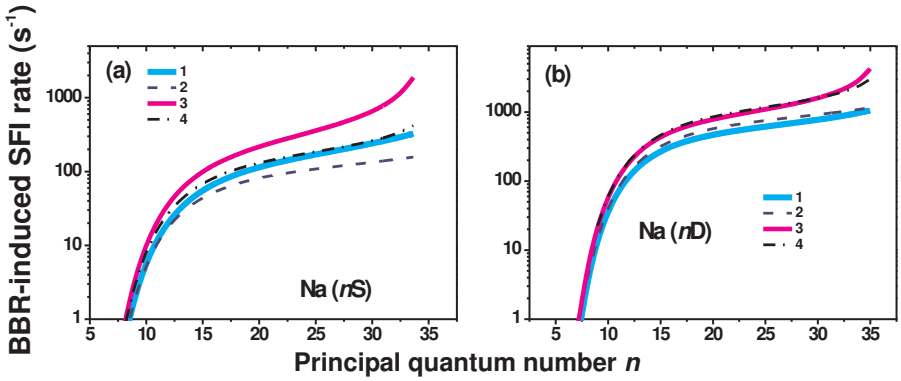

Figure 9. Calculated BBR-induced SFI rates W_{SFI} for (a) nS and (b) nD Rydberg states of sodium at the ambient temperature of 300 K. Curves (1) and (3) are numerical results obtained using the Dyachkov and Pankratov model at the electric-field amplitudes of E=100 and 200 V/cm, respectively. Curves (2) and (4) are analytical results obtained using equation (30) at the electric-field amplitudes of E=100 and 200 V/cm, respectively.

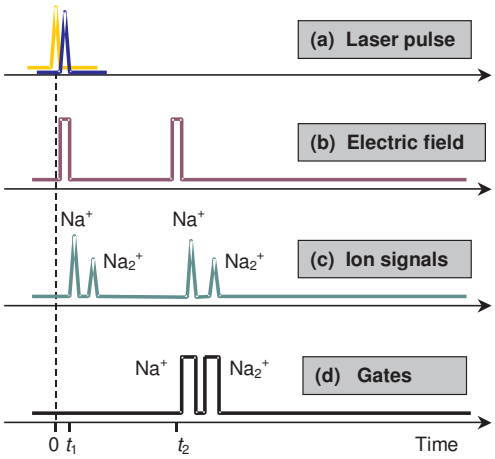

Figure 10. Timing diagram of the experiment: (a) laser excitation pulse; (b) electric field pulses for the ion extraction; (c) atomic A^+ and molecular A_2^+ ion signals; (d) detector gates.

where $A(nS \rightarrow n'P)$ and $W(nS \rightarrow n'P)$ are the rates of population of $n'P$ states due to spontaneous transitions and BBR-induced transitions from the initial nS state, respectively, and $\tau_{eff}^{n'P}$ is the effective lifetime of the $n'P$ state.

A combination of equation (34) with equations (31) and (32) yields

$$W_{BBR}^{mix}(nS) = \sum_{n'} \frac{\left[W(nS \rightarrow n'P) + A(nS \rightarrow n'P)\right] W_{BBR}(n'P)}{1/\tau_{eff}^{n'P} - 1/\tau_{eff}^{nS}} \times \left(1 - \frac{t_{eff}^{nS}}{t_{eff}^{n'P}}\right). \quad (35)$$

The main contribution to the sum in equation (35) is from $n'P$ states with $n' = n \pm 1$ [see figure 1(b)].

The effective BBR-induced ionization rates for nP and nD states are determined in the same way as for nS states, taking into account the population transfer to both $n'(L+1)$ and $n'(L-1)$ states.

The rate W_{SFI}^{mix} describes the second-order process - BBR-induced transitions from the neighboring $n'L'$ states to highly excited states $n''L''$ with $n'' > n_c$ [see figure 1(a)], followed by ionization of these states by extraction electric field pulses. This rate is also calculated using equation (35), in which W_{BBR} is replaced by W_{SFI} and the summation is done over the states with $n' < n_c$.

Figures 11-13 show the results of numerical calculations of total ionization rates W_{BBR}^{tot} of nS, nP, and nD Rydberg states of alkali-metal atoms. The calculations were done for a broad range of principal quantum numbers (n=8-65) and temperatures (T = 77, 300, 600 K), at the amplitudes of extraction electric field of 5 V/cm (solid curves) and 10 V/cm (dashed curves). For comparison, the direct BBR-induced ionization rates are also shown (dash-dotted curves).

The values of W_{BBR}^{tot} depend on the time interval of accumulation of ions in the interaction region. For sodium and rubidium atoms, the calculations were made for $t_1 = 0.3$ μs and $t_2 = 2.1$ μs, which corresponds to the conditions of our experiment described in Section 3. For lithium, potassium and cesium atoms for the sake of simplicity we used $t_1 = 0$ μs and $t_2 = 2$ μs. Such choice of the time interval does not noticeably change the calculated rates; it is important only for the states with low $n \sim 10$ with short lifetimes ~ 1 μs. The effective lifetimes of Rydberg states, which are necessary for the determination of t_{eff} , were calculated using the Dyachkov and Pankratov formulas for radial matrix elements [60].

Figure 11(a) shows the calculated total BBR-induced ionization rates for lithium nS Rydberg states. Account for BBR-induced mixing leads to a strong increase of the total BBR-induced ionization rate. In contrast, the rate of the direct BBR-induced photoionization of lithium nP Rydberg states is by two orders of magnitude larger than the direct BBR-induced rate for nS states, and the main contribution to the total number of ions is due to the $n'P$ states with $n' = n \pm 1$. Taking into account the SFI of high-lying Rydberg states and photoionization of neighboring Rydberg states by BBR substantially alters both the absolute values of W_{BBR}^{tot} and the shapes of their dependences on n. In the case of sodium, potassium, rubidium, and cesium Rydberg states (figures 11-13) the difference between the direct BBR-induced photoionization rates and the total BBR-induced ionization rates is smaller, but remains observable.

3. Experimental study of BBR-induced ionization

3.1. Temperature dependence of BBR-induced ionization rate

The temperature dependence of BBR-induced ionization rate of the sodium $17D$ Rydberg atoms was measured by Spencer et al. [10]. The measurements were performed in an effusive beam of sodium atoms which passed through a thermally controlled interaction region. The atoms were excited to the $17D$ state by two pulsed dye lasers. The laser beams were collinear with the atomic beam and excitation took place between two electric-field plates in a cryogenic environment. After a delay of 500 ns, a small electric field of 8 V/cm was applied to guide the ions from the interaction region through a small hole in the lower field plate to the electron multiplier. The 500 ns interval was sufficiently short to ensure that BBR-induced transitions to neighboring $n'P$ and $n'F$ levels did not affect the results of measurements.

The temperature was varied in the range 90-300 K by pouring measured amounts of liquid nitrogen into the cryostat and allowing it to boil off. Although the cryostat rapidly equilibrated to the new temperature, a thermal drift limited the useful observation time to about 15 minutes for each data point, so that there were about 1800 data pulses at each temperature. The number density of excited atoms was less than $10^5\,\mathrm{cm}^{-3}$, low enough to avoid Rydberg-Rydberg collisions and superradiant transfer between Rydberg states. The background pressure was less than 10^{-7} Torr, sufficiently small to avoid also

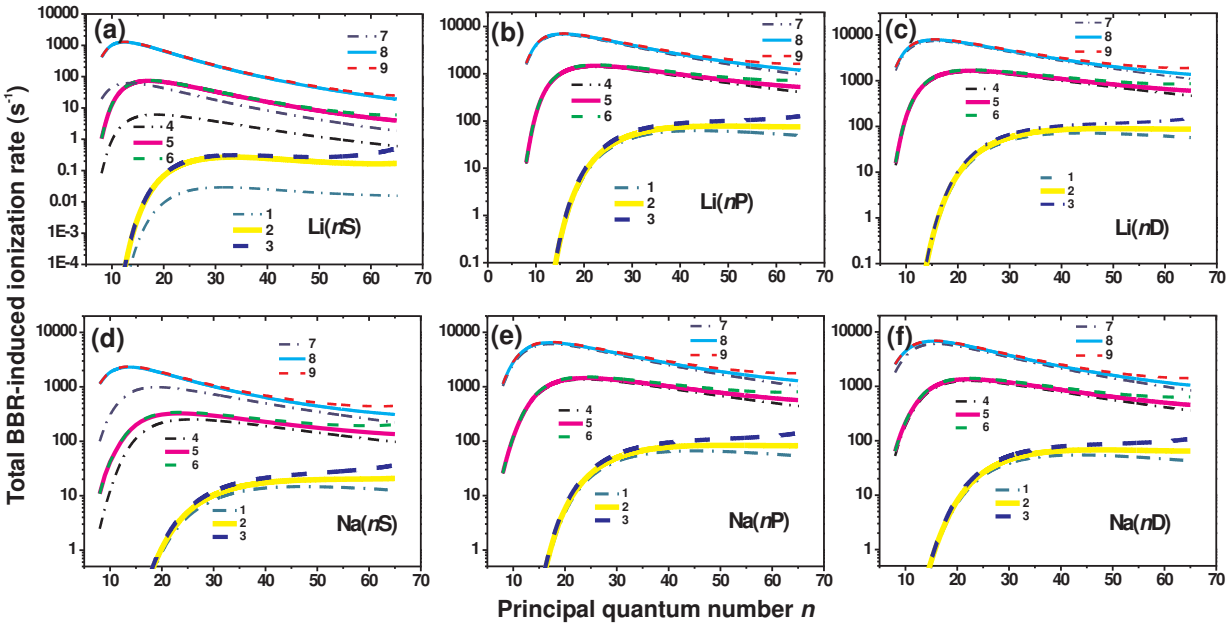

Figure 11. Calculated total BBR-induced ionization rates W_{BBR}^{tot} for (a) nS, (b) nP, (c) nD Rydberg states of lithium and (d) nS, (e) nP, and (d) nD Rydberg states of sodium. Curves (1), (4), and (7) are the direct BBR-induced photoionization rates at the ambient temperatures of T=77, 300, and 600 K, respectively. Curves (2), (5), and (8) are the total BBR-induced ionization rates at the amplitude of extraction electric field pulses of E=5 V/cm for ambient temperatures of T=77, 300, and 600 K, respectively. Curves (3), (6), and (9) are the total BBR-induced ionization rates at the amplitude of extraction electric-field pulses of E=10 V/cm for ambient temperatures of T=77, 300, and 600 K respectively.

collisions with background gases. The absolute collisional ionization rates were not measured, but the experimental points were normalized to the theory.

The three sources of possible uncertainties were considered by the authors. The first one was a counting statistics, the other ones were the fluctuations of the intensity of laser radiation, responsible for errors of 2-3% at each data point, and the last one was a drift of the temperature of the vacuum chamber, which led to error of $\pm 5\,\mathrm{s}^{-1}$ for each data point.

A systematic shift due to an extracting field was considered. The 8 V/cm field ionized all states with $n > 80$ (see Section 2). The calculated rate of BBR-induced transfer to states with $n > 80$ was so small that it could be neglected. However, an increase of the amplitude to several hundred V/cm, required to ionize the states with $n > 30$, led to a significant increase of the measured signal, which was consistent with the results of the calculation of the BBR-induced transfer rates to states with $n > 30$.

BBR-induced ionization occurs due to photons of shorter wavelength than those which cause transitions to neighboring Rydberg states. Hence, a measurement of BBR-induced ionization rates instead of discrete transition rates can be a stricter test of the

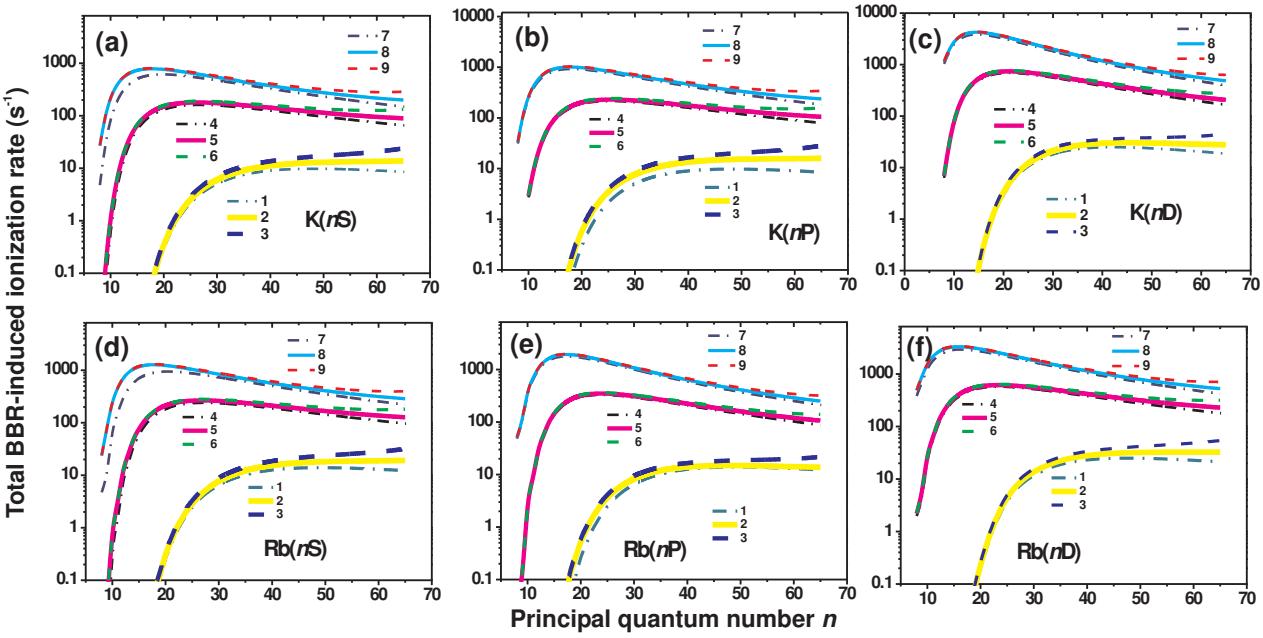

Figure 12. Calculated total BBR-induced ionization rates W_{BBR}^{tot} for (a) nS, (b) nP, and (c) nD Rydberg states of potassium, and (d) nS, (e) nP, and (d) nD Rydberg states of rubidium. Curves (1), (4), (7) are the direct BBR-induced photoionization rates for ambient temperatures of T=77, 300, and 600 K, respectively. Curves (2), (5), (8) are the total BBR-induced ionization rates at the amplitude of extraction electric field pulses of E=5 V/cm and ambient temperatures of T=77, 300, and 600 K respectively. Curves (3), (6), (9) are the total BBR-induced ionization rates at the amplitude of extraction electric field pulses of E=10 V/cm and ambient temperatures of T=77, 300, and 600 K, respectively.

temperature of blackbody radiation. In ref. [10], the photoionization became observable at 100 K due to 1% parasitic contribution from 300 K blackbody radiation. Based on the apparatus size and the emissivity of the materials surrounding the interaction region, it was estimated that less than 0.4% of a 300 K radiation existed within the interaction region. Finally, the measured photoionization rate varied by a factor greater than 100 over the temperature range 77-300 K studied, and a good agreement between experiment and theory was observed.

3.2. Experimental study of the dependence of ionization rates on n.

Burkhardt et al. [12] studied the ionization of sodium Rydberg atoms in a gas cell at the temperature of 500 K. The atoms were excited to Rydberg nS and nD states with $18 \leq n \leq 35$ by a pulsed dye laser. The dependences of the ionization signals on the principal quantum number were measured. It has been shown that at the number density of ground-state atoms $n_{3S} \sim 10^{11}\,\mathrm{cm}^{-3}$ the photoionization by blackbody radiation was a predominant source of atomic ions, and contribution from collisional ionization could

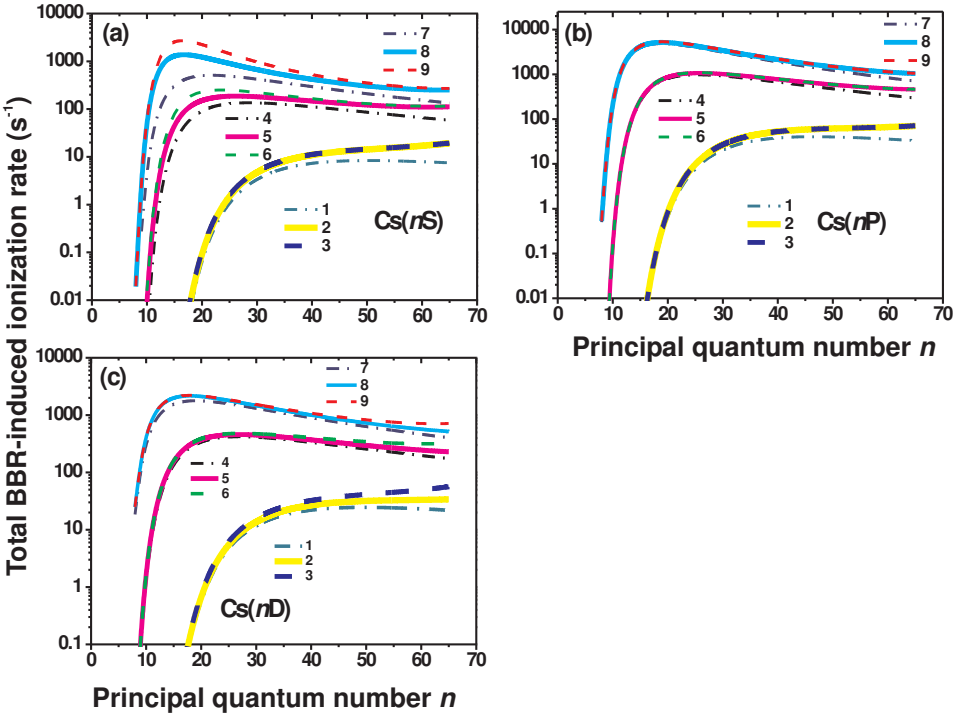

Figure 13. Calculated total BBR-induced ionization rates W_{BBR}^{tot} for (a) nS, (b) nP, and (c) nD Rydberg states of cesium. Curves (1), (4), (7) are the direct BBR-induced photoionization rates for ambient temperatures of T=77, 300, and 600 K, respectively. Curves (2), (5), (8) are the total BBR-induced ionization rates at the amplitude of extraction electric field pulses of E=5 V/cm for ambient temperatures of T=77, 300, and 600 K, respectively. Curves (3), (6), (9) are the total BBR-induced ionization rates at the amplitude of extraction electric-field pulses of E=10 V/cm for ambient temperatures of T=77, 300, and 600 K, respectively.

be neglected.

Allegrini et al. [61] studied collisional mixing of Ba Rydberg states. The signal of BBR-induced ionization was used to measure the relative population of barium Rydberg states, instead of the commonly used SFI method. The number density of ground-state atoms in the experiment was close to $10^{12}\,\mathrm{cm}^{-3}$. At this density the method of SFI is inapplicable due to electric breakdown. The simple formula (17) was used to calculate the rate of BBR-induced ionization.

The dependence of associative and BBR-induced ionization rates of the sodium nS and nD Rydberg atoms with n=8-20 on the principal quantum number n was measured by us in [29]. Experiments were performed using a single effusive Na atomic beam in a vacuum chamber at the background pressure of 5×10^{-7} Torr (figure 14). The temperature of the Na oven was stabilized at 635 K. The atomic beam was formed by an expansion of sodium vapor through a 2 mm diameter opening in the oven at a distance of 9 cm from the reaction zone. Collimation of the beam was achieved by a 1.5 mm diameter aperture, located 4 cm upstream from the reaction zone. The effective

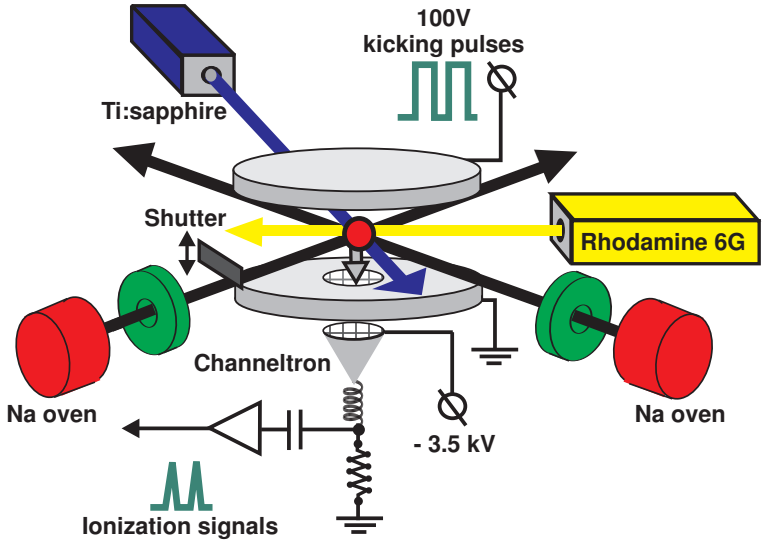

Figure 14. Experimental arrangement of the atomic and laser beams, and the ion detection system.

diameter of the atomic beam in the reaction zone was about 4 mm.

Sodium nS and nD Rydberg states were excited using the two-step scheme $3S_{1/2} \rightarrow 3P_{3/2} \rightarrow nS, nD$ by radiations of two tunable lasers pulsed at a 5 kHz repetition rate. In the first step, 50 ns pulses from a Rhodamine 6G dye-laser with linewidth of 50 GHz were used. They saturated the $3S_{1/2} \rightarrow 3P_{3/2}$ transition at 589 nm (*yellow*). The resonance fluorescence on this transition was detected by a photomultiplier to monitor the relative changes in the number density of the atomic beam. In the second step, the second harmonic of a Ti-sapphire laser was used. It yielded 50 ns pulses with 10 GHz linewidth, tunable in the 400-430 nm range (*blue*). When not focused, this radiation did not saturate the $3P_{3/2} \rightarrow nS, nD$ transitions. The two laser beams were crossed at a right angle in the reaction zone, both of them crossing the atomic beam at a 45° angle. Laser beams were spatially limited by 2 mm diameter apertures at the entrance windows of the vacuum chamber. Such configuration ensured a sufficiently small excitation volume of 2 mm size in the central part of the atomic beam, where the spatial variation of atom number density was insignificant ($< 20\%$).

The ion detection system shown in figure 14 used a channeltron multiplier VEU-6. The atomic beam passed between two stainless-steel plates with diameter of 70 mm, spaced by 10 mm. The plates formed a homogeneous electric field to guide the ions from the reaction zone through the entrance window of the channeltron. The extraction electric field pulses of 100 V/cm amplitude and 250 ns duration were applied to the upper plate. The lower plate was grounded and had a 6 mm diameter opening covered by a mesh with the transmittance of 70%. The ions that passed through the mesh were accelerated by the electric field of the channeltron to energies of about 3.5 keV.

Single ion output pulses of the channeltron were amplified, discriminated, and registered by two gated counters. The measurements were performed in the pulse

counting regime, keeping the frequencies of the detected ion signals much lower (0.2-1 kHz) than the 5 kHz repetition rate of laser pulses. Less than one ion per laser shot was detected on average. The measured frequencies of ion signals were determined as the total number of ions detected during the measurement time of 10 s, i.e., signals were counted for 50000 laser pulses. In order to ensure the single-ion counting regime, the intensity of the laser driving the second excitation step was attenuated with calibrated neutral density filters by a factor of 10 to 100.

Our experimental study concentrated on measurements of relative dependences of ionization rates on the principal quantum number n of Rydberg states, and did not require precise absolute values of the number density n_{3S} of the ground-state Na($3S$) atoms in the atomic beam. The number density n_{3S} in the reaction zone was calculated using a recent and reliable formula by Browning and Potter [62], and it was estimated to be $n_{3S} = (5 \pm 1) \times 10^{10}$ cm^{-3} at the oven temperature of $T = (635 \pm 2)$ K. Monitoring of the fluorescence on the saturated resonance transition showed that the atomic number density was almost constant during the experiments.

The time sequence of excitation and detection pulses is illustrated in figure 10. The first electric field pulse cleaned the reaction zone from the undesirable atomic and molecular ions, arisen from photoionization of Rydberg atoms by laser radiation and photoassociative ionization of sodium $3P$ atoms [63, 64], respectively.

After the second electric field pulse, the registered Na^+ and Na_2^+ ion signals resulted from ionization occurring in the reaction zone during the time interval $t_2 - t_1 = 1.8$ μs between the two extraction electric field pulses. This time is comparable with the lifetimes of Rydberg states; therefore, time evolution of ionization processes must be analyzed. The main processes leading to the production of Na^+ ions are Penning-type ionization (PI) and photoionization by BBR. The Na_2^+ ions can be created only in the associative ionization (AI). Associative ionization is the simplest two-body collision, leading to formation of a chemical bond. A Rydberg atom A(nL) collides with the ground-state atom A in the reactions:

$$\begin{aligned} &\mathrm{A}\,(nL) + \mathrm{A} \rightarrow \mathrm{A}_2^+ + e^- \qquad \text{(AI)} \\ &\mathrm{A}\,(nL) + \mathrm{A} \rightarrow \mathrm{A}^+ + \mathrm{A} + e^- \qquad \text{(PI)} \end{aligned}$$

A contribution of the collisions with background gases can be safely disregarded. We have verified experimentally that the variation of background pressure within the range of $5{\times}10^{-7} \leq \mathrm{P} \leq 1 \times 10^{-6}$ Torr did not affect the measured Na^+ and Na_2^+ signals by more than 5%. Under such conditions, the rate equations describing the evolution of the number of Na^+ and Na_2^+ ions following the laser excitation at time t=0 are [see equation (31)]

$$\begin{cases} \dfrac{d\mathrm{Na}^+(t)}{dt} = k_{PI} N_{nL}\,(t)\ n_{3S} + W_{BBR} N_{nL}\,(t)\,; \\ \\ \dfrac{d\mathrm{Na}_2^+(t)}{dt} = k_{AI} N_{nL}\,(t)\ \ n_{3S}. \end{cases} \tag{36}$$

Here $N_{nL}\,(t) \approx N_{nL}\,(0)\ \exp\left[-t/\tau_{eff}\right]$ is the time-dependent number of Na(nL) Rydberg

atoms in the reaction zone, $n_{3S} = 5 \times 10^{10}$ cm^{-3} is the number density of ground state atoms, k_{AI} and k_{PI} are rate constants of associative and Penning ionization in Na(nL)+Na($3S$) collisions. The initial number of Rydberg atoms, $N_{nL}(0)$, created during laser excitation can be written as

$$N_{nL}(0) = N_{3P} W\left(3P_{3/2} \rightarrow nL\right), \tag{37}$$

where N_{3P} is the average number of atoms in the $3P_{3/2}$ state during the yellow-laser pulse, and $W\left(3P_{3/2} \rightarrow nL\right)$ is the probability of excitation of the Na($3P_{3/2}$) atoms to the nL state by a single blue-laser shot.

The effective lifetime τ_{eff} describing the decay of Rydberg states in equation (10) is determined by the spontaneous lifetime and the rate of other processes depleting the laser excited Rydberg state. These include BBR induced transitions between Rydberg states, BBR induced photoionization, and collisional quenching.

The depletion of Rydberg states with n=8-20 by collisional ionization is negligible at the atom density used in our experiment. According to our estimates, the rate of associative ionization, $k_{AI} n_{3S}$, does not exceed 50 s^{-1} and is therefore much smaller than the spontaneous decay rates, which range from 10^5 to 10^6 s^{-1} for the studied Rydberg states. The rate of PI, $k_{PI} n_{3S}$, is expected to be below 10 s^{-1} for $n \sim$20, and close to zero for lower n. Comparing the PI rate with the direct BBR photoionization rate W_{BBR}, one can see that Na^+ ions are produced mainly via BBR photoionization. As will be shown below, this background ionization process can be favorably exploited for the determination of absolute AI rate constants.

With the above considerations in mind, the solution of equations (36) can be written as

$$\begin{cases} Na^+ = N_{nL}(0)\ W_{BBR}\ t_{eff} \\ Na_2^+ = N_{nL}(0)\, k_{AI} n_{3S}\ t_{eff} \end{cases} \tag{38}$$

where t_{eff} is the effective time of interaction that takes into account the short radiative lifetimes of Rydberg states, determined by equation (33)

Equations (38) can be used for a direct measurement of k_{AI} and W_{BBR} values, provided $N_{nL}(0)$ is known. The only reliable method to measure $N_{nL}(0)$ is the SFI technique. Unfortunately, SFI method is difficult to apply to Rydberg states with low n, since it requires too strong electric field ($\sim$30 kV/cm for $n \sim 10$).

On the other hand, we were interested mainly in relative measurements of W_{BBR} for various n. Therefore we could use a normalization procedure for $N_{nL}(0)$ based on numerically calculated excitation probabilities $W\left(3P_{3/2} \rightarrow nL\right)$. Since the $3S_{1/2} \rightarrow 3P_{3/2}$ transition was saturated, $N_{nL}(0)$ depended only on the respective transition moments and power of the blue laser. In the absence of saturation at the second excitation step (this was the case for our experiments), the probability of excitation of Rydberg states from the $3P_{3/2}$ state can be written as

$$W\left(3P_{3/2} \rightarrow nL\right) = C_L \cdot I_b \cdot R^2\left(3P_{3/2} \rightarrow nL\right), \tag{39}$$

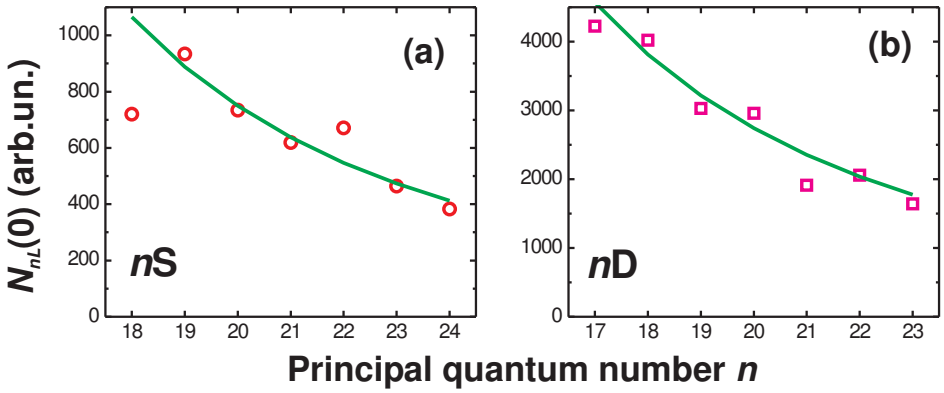

Figure 15. Relative probabilities of laser excitation of sodium Rydberg states: (a) nS states; (b) nD states. Open circles and squares - experiment, solid curves - theory.

where I_b is the power of the blue laser, $R\left(3P_{3/2} \rightarrow nL\right)$ is the radial part of the transition dipole moment, and C_L is a normalization constant which depends on L and is proportional to the square of angular part of the matrix element. $W\left(3P_{3/2} \rightarrow nL\right)$ falls as n_{eff}^{-3} for high Rydberg states, but for the states with $n \sim 10$ this scaling low does not work well. We have revealed this fact in our numeric calculations of $R\left(3P_{3/2} \rightarrow nL\right)$ for the $3P_{3/2} \rightarrow nS, nD$ transitions, and therefore used the numerical data in subsequent measurements instead of the scaling law.

In order to compare the absolute signals due to BBR and collisional ionization of nS and nD states, it is necessary to know also the ratio C_D/C_S. The analysis of angular parts of the transition matrix elements, taking into account the hyperfine structure, has shown that for excitation with linearly polarized light in the first and the second excitation steps, the ratio C_D/C_S may vary from approximately 1.6 (if there is no collisional, radiative, or magnetic field mixing of the magnetic sublevels) to 2 (if the sublevel mixing is complete). For excitation by non-polarized light, the ratio always equals to 2 regardless the degree of level mixing. Finally, we find that the ratio $W\left(3P_{3/2} \rightarrow nD\right)/W\left(3P_{3/2} \rightarrow nS\right)$ may vary between the 3.5 and 5.

In principle, one could normalize the ion signals measured for different nL states using the calculated probabilities $W\left(3P_{3/2} \rightarrow nL\right)$ and measuring only the power I_b of the blue laser radiation and equation (39). However, the applicability of such normalization may be complicated by technical imperfections of the blue laser. Since the linewidth of this laser (10 GHz) was much larger than the widths of the absorption profiles at the second excitation step (∼500 MHz Doppler broadening), variations of the spectral density of laser radiation could affect the probability of excitation even if I_b would be kept constant. Therefore we had to verify experimentally the applicability of normalization by equation (39). As discussed above, the only reliable way to measure the number of Rydberg atoms was to apply the SFI technique. For this purpose, we built a high-voltage generator yielding pulses with rise time of 1 μs and amplitude of

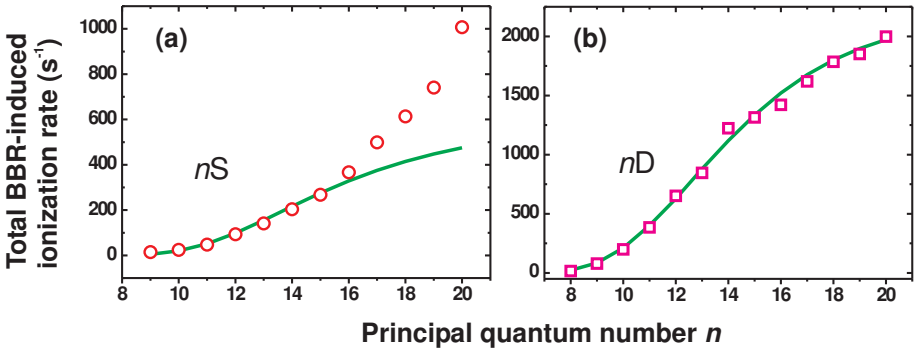

Figure 16. Total BBR induced ionization rates for (a) nS states and (b) nD sodium Rydberg states. Open circles and squares - experiment, solid lines - theory.

up to 8 kV. This allowed us to field-ionize Rydberg states with $n \geq 17$. The SFI signals were detected at a 1 μs delay with respect to the laser pulse, i.e., the measured SFI signal was:

$$S_{SFI} \sim N_{nL}\,(0)\,\exp\left(-1\ \mu\mathrm{s}/\tau_{eff}\right). \tag{40}$$

Equation (40) was used to derive $N_{nL}(0)$ from the measured SFI signals and the calculated values of τ_{eff}, which were published in Ref. [60]. Figure 15 shows the measured $N_{nL}(0)$ dependences on the principal quantum number n for nS and nD states. These data are normalized over I_b, because it varied as the blue laser frequency was tuned to resonance with different nL states. The solid curves are the approximations made using equation (39). It is seen that experimental points have noticeable deviations from theory although the general trend is correct. These deviations may be explained by the variations of spectral density of the blue laser light. We concluded that equation (39) can be used for the normalization of $N_{nL}(0)$, but at a price of limited accuracy. We also find from figure 15 that average ratio $W(3P_{3/2} \rightarrow nD)/W(3P_{3/2} \rightarrow nS)$ was close to 3.5. Hence, no considerable mixing of the magnetic sublevels took place during laser excitation, and the ratio C_D/C_S was close to 1.6.

Experimental and theoretical data on the total Na BBR ionization rates at T=300 K are compared in figure 16. The solid curves are the theoretical values of W^{tot}_{BBR} (see Section 2). The squares and circles are the corresponding experimental values W^{exp}_{BBR} obtained with equations (38) and (39) [in equation (38) the value of W_{BBR} was replaced with W^{tot}_{BBR}]. Experimental data were averaged over 5 measurements. The normalization coefficient C_D in equation (39) was the only free parameter whose absolute value was adjusted to fit experiment and theory. A remarkably good agreement between the experimental and theoretical data was found for nD states [figure 16(a)]. At the same time, the data for nS states, obtained with measured earlier ratio $C_D/C_S = 1.6$, exhibit considerable discrepancies for states with higher n [figure 16(b)], while the agreement for states with lower n is much better. The values of W^{exp}_{BBR} exceed the values of W^{tot}_{BBR}

by 2.1 times for n=20, and the shape of the experimental n dependence was significantly different from the theoretical one.

One possible explanation of anomaly for nS states is related to their specific orbit that penetrates into the atomic core. The penetration causes a strong interaction between the Rydberg electron and the core, e.g., due to core polarization [47]. This results in a large quantum defect and a Cooper minimum in the photoionization cross-sections. This assumption is supported by the good agreement of theory and experiment for the hydrogen-like nD states, which have a small quantum defect and almost non-penetrating orbits.

3.3. Application to measurements of collisional ionization rates

Since SFI technique was not applicable for direct determination of $N_{nL}(0)$ for n=8-17, and the use of equation (40) was seen to be somewhat inadequate in our experiment, we had to find a way to eliminate this value in the measurements. We decided to measure the ratio R of atomic and molecular signals derived from equations (38):

$$R = \frac{\mathrm{Na}_2^+}{\mathrm{Na}^+} = \frac{k_{AI}\mathrm{n}_{3S}}{W_{BBR}^{tot}}. \tag{41}$$

This ratio is independent of the values of $N_{nL}(0)$, τ_{eff} and t_{eff}. Thus, the rate constant of the AI process can be directly obtained from the measured ratio of the Na_2^+ and Na^+ signals:

$$k_{AI} = \frac{\mathrm{Na}_2^+}{\mathrm{Na}^+} \cdot \frac{W_{BBR}^{tot}}{\mathrm{n}_{3S}}. \tag{42}$$

The BBR ionization rates W_{BBR} became to be key values necessary for the determination of the AI rate constants. Therefore, an accuracy with which the W_{BBR} values are known determines the accuracy of the experimental k_{AI} values obtained with equaiton (42).

In our experiments associative ionization rate constants were measured separately in single and crossed Na atomic beams at temperatures of T=635 K (single beam) and T=600 K (crossed beams). The results of these measurements were published in our previous works [29, 65].

3.4. Experimental studies of ultracold plasma

The mechanism of formation of an ultracold plasma from a dense sample of cold Rydberg atoms was briefly described in the Introduction. Roughly 2/3 of Rydberg atoms are converted into a plasma, while the remaining atoms decay to low-lying states, thus keeping the energy balance.

Spontaneous evolution of cold Rydberg atoms into ultracold plasma was first observed by Robinson et al. [16]. Experiments were performed with Rb and Cs Rydberg atoms held in a magneto-optical trap (MOT). The cloud of cold atoms had a temperature of 300 μK in the case of rubidium, and 140 μK in the case of cesium. The atoms were excited from the $5P_{3/2}$(Rb) or $6P_{3/2}$(Cs) states to the Rydberg states by radiations

of the pulsed dye lasers. Untrapped room-temperature atoms were also excited into Rydberg states, which made 1% contribution to the total number of excited Rydberg atoms. At delay time t_d after the laser pulse, a rising voltage pulse was applied to the parallel electric-field plates surrounding the excitation volume. The time t_d was varied in the interval 0-50 μs. The rising pulse first frees electrons bound to the plasma, then ionizes Rydberg atoms and drives electrons (or ions, depending on the polarity) to a microchannel-plate detector (MCP). The time resolved ionization signals were studied. A plasma signal, which came before the field ionization pulses, was observed even at delay times $t_d = 20$ μs, which observation demonstrated that Rydberg atoms had evolved into a plasma.

Later, Gallagher et al. [25, 26] studied the role of dipole-dipole interaction for the ionization of ultracold Rydberg gas. It has been shown that for Rydberg states with $n < 40$ BBR and collisions are the predominant sources of initial ionization, but for higher states ionization is caused mostly by the resonant dipole interaction of Rydberg atoms. These results show that accurate calculations and experimental measurements of the rates of BBR-induced and collisional ionization are of great importance for contemporary studies of the formation of ultracold plasma.

4. Conclusion

We have calculated the total BBR-induced ionization rates of nS, nP and nD Rydberg states of all alkali-metal atoms for principal quantum numbers n=8-65 at the ambient temperatures of 77, 300 and 600 K. Our calculations take into account the effect of BBR-induced mixing of Rydberg states and their field ionization by extracting electric field pulses. Useful analytical formulas have been derived, which allow for quick estimation of ionization rates and their dependences on the principal quantum number n. The numerical results are in a good agreement with our recent experiment data on Na nS and nD states, except for nS states with $n > 15$, which is most probably associated with the Cooper minimum in the photoionization cross-section.

The obtained results show that BBR-induced redistribution of population over Rydberg states and their field ionization by extracting electric fields affect both the magnitudes of the total ionization rates and shapes of their dependences on the principal quantum number. This suggests that these processes are important and cannot be ignored in the calculations and measurements of BBR ionization rates. Equations (31)-(35), as well as the analytical formulas (27) and (30), can be used to calculate the total ionization rates W_{BBR}^{tot} under particular experimental conditions. The numerical results presented in figures 3-13 may be helpful to the analysis of ionization signals measured in experiments on collisional ionization and spontaneous formation of ultracold plasma, since BBR-induced ionization is the main source of atomic ions. New experimental data for alkali-metal Rydberg atoms in a broader range of principal quantum numbers would be of interest for the further improvement of theory, especially for the non-hydrogen-like states.

The set of results obtained by us constitutes the first systematic study of BBR-induced ionization of all alkali-metal Rydberg atoms. It may be helpful in the analysis of the mechanism of ultracold plasma formation in different experimental conditions [16, 19].

5. Acknowledgments

This work was supported by the Russian Academy of Science, Dynasty Foundation, EU FP6 TOK Project LAMOL (Contract MTKD-CT-2004-014228), Latvian Science Council and European Social Fund.

6. References

[1] Smoot G F , Gorenstein M V and Muller R A 1977 *Phys. Rev. Lett.* **39** 898
[2] Gallagher T F and Cooke W E 1979 *Phys. Rev. Lett.* **42** 835
[3] Gallagher T F and Cooke W E 1979 *Phys. Rev. A* **20** 670
[4] Cooke W E and Gallagher T F 1980 *Phys. Rev. A* **21** 588
[5] Hildebrandt G F, Beiting E J, Higgs C, Hatton G J, Smith K A, Dunning F B and Stebbins R F 1981 *Phys. Rev. A* **23** 2978
[6] Spencer W P, Waidyanathan A G, Kleppner D, Ducas T W 1981 *Phys. Rev. A* **24** 2513
[7] Spencer W P, Waidyanathan A G, Kleppner D, Ducas T W 1982 *Phys. Rev. A* **25** 380
[8] Theodosiou C E 1984 *Phys. Rev. A* **30** 2881
[9] Farley J W, Wing W H 1981 *Phys. Rev. A* **23** 2397
[10] Spencer W P, Vaidyanathan A G, Kleppner D, Ducas T W 1982 *Phys. Rev. A* **26** 1490
[11] Lehman G W 1983 *Phys. Rev. A* **16** 2145
[12] Burkhardt C E, Corey R L, Garver W P, Leventhal J J, Allegrini M, Moi L 1986 *Phys. Rev. A* **34** 80
[13] Hill S B, Parsasarathy R, Suess L and Dunning F B 2000 *Phys. Rev. A* **62** 015403
[14] Galvez E J, Lewis J R, Chaudhuri B, Rasweiler J J, Latvakoski H, DeZela F, Massoni E, and Castillo H 1995 *Phys. Rev. A* **51** 4010
[15] Galvez E J, MacGregor C W, Chaudhuri B, Gupta S, Massoni E, and DeZela F 1997 *Phys. Rev. A* **55** 3002
[16] Robinson M P, Tolra B L, Noel M W, Gallagher T F and Pillet P 2000 *Phys. Rev. Lett.* **85** 4466
[17] Killian T C, Kulin S, Bergeson S D, Orozco L A, Orzel C, and Rolston S L 1999 *Phys. Rev. Lett.* **83** 4476
[18] Killian T C, Lim M J, Kulin S, Dumke R, Bergeson S D, and Rolston S L 2001 *Phys. Rev. Lett.* **86** 3759
[19] Li W, Noel M W, Robinson M P, Tanner P J, Gallagher T F, Comparat D, Tolra B L, Vanhaecke N, Vogt T, Zahzam N, Pillet P, Tate D A 2004 *Phys. Rev. A* **70** 042713
[20] Pohl T, Pattard T, and Rost J M 2003 *Phys. Rev. A* **68** 010703
[21] Pohl T, Pattard T, and Rost J M 2004 *Phys. Rev. A* **70** 033416
[22] Roberts J L, Fertig C D, Lim M J, and Rolston S L 2004 *Phys. Rev. Lett.* **92** 253003
[23] Vanhaecke N, Comparat D, Tate D A, and Pillet P 2005 *Phys. Rev. A* **71** 013416
[24] Li W, Tanner P J, and Gallagher T F 2005 *Phys. Rev. Lett.* **94** 173001
[25] Li W, Tanner P J, Jamil Y, and Gallagher T F 2006 *Eur. Phys. J. D* **40** 27
[26] *Topical issue on ultracold plasmas and cold Rydberg atoms* edited by Pillet P and Comparat D 2006 *Eur. Phys. J. D* **40** 1
[27] Fletcher R S, Zhang X L, and Rolston S L 2007 *Phys. Rev. A* **78** 145001

[28] Viteau M, Chotia A, Comparat D, Tate D A, Gallagher T F, and Pillet P 2008 *Phys. Rev. Lett.* **99** 040704
[29] Ryabtsev I I, Tretyakov D B, Beterov I I, Bezuglov N N, Miculis K and Ekers A 2005 *J. Phys. B: At. Mol. Opt. Phys.* **38** S17
[30] Stebbings R F, Latimer C J, West W P, Dunning F B and Cook T B 1975 *Phys. Rev. A* **12** 1453; Ducas T, Littman M G, Freeman R R and Kleppner D 1975 *Phys. Rev. Lett.* **35** 366; Gallagher T F, Humphrey L M, Hill R M and Edelstein S A 1976 *Phys. Rev. Lett.* **37** 1465
[31] Beterov I I, Tretyakov D B, Ryabtsev I I, Ekers A, Bezuglov N N 2007 *Phys. Rev. A* **75** 052720
[32] Beterov I I, Ryabtsev I I, Tretyakov D B, Bezuglov N N, Ekers A 2008 Sov. Phys. JETP **107** 20
[33] Beterov I I, Ryabtsev I I, Tretyakov D B, Entin V M 2008 *Vestnik NGU: Fizika (Bulletin of Novosibirsk State University, Physics)* **3** 84 (in Russian)
[34] *Rydberg States of Atoms and Molecules*, edited by Stebbins R F and Dunning F B 1983 (Cambridge University, Cambridge, New York)
[35] Gallagher T F *Rydberg atoms* 1994 (Cambridge University Press, Cambridge).
[36] Gallagher T F *Rydberg atoms* 1988 *Rep.Prog.Phys.* **51** 143
[37] Filipovicz P, Meystre P, Rempe G and Walther H, 1985 *Optica Acta* **32** 1105
[38] Haroche S, Fabre C, Goy M, Gross M, Raimond J M, *Laser Spectroscopy IV, Springer Series in Optical Sciences* 1979 (Edited by Walther H and Rothe K W, Berlin, Springer-Verlag) **21** 244.
[39] Beiting E J, Hildebrandt G F, Kellert F G, Foltz G W, Smith K A, Dunning F B, Stebbins R F 1979 *J. Chem. Phys.* **70** 3551
[40] Zimmerman M L, Littman M G, Kash M M, Kleppner D 1979 *Phys. Rev. A* **20** 2251
[41] Van Regermorter H, Hoang Bing Dy, Prud'homme M, 1979 *J. Phys. B: At. Mol. Phys.* **12** 1053
[42] Glukhov I L and Ovsiannikov V D 2007 *Proc. SPIE* **6726** 67261F
[43] Dyachkov L G and Pankratov P M, 1991 *J. Phys. B: At. Mol. Opt. Phys.* **24** 2267
[44] Dyachkov L G, Pankratov P M 1994 *J. Phys. B: At. Mol. Opt. Phys.* **27** 461
[45] Goreslavsky S P, Delone N B and Krainov V P 1982 *Sov. Phys. JETP*, **55** 246
[46] Davydkin V A and Zon B A 1981 *Opt. Spectr.* **51** 13
[47] Aymar M 1978 *J. Phys. B* **11** 1413
[48] Delone N B, Goreslavsky S P, and Krainov V P 1989 *J. Phys. B: At. Mol. Opt. Phys.* **22** 2941
[49] Rau A R P and Inokuti M 1997 *Am. J. Phys.* **65** 221
[50] Hartree D 1928 *Proc. Cambridge Philos. Soc.* **24** 426
[51] Stevens G D, Iu C H, Bergeman T, Metcalf H J, Seipp I, Taylor K T, Delande D 1996 *Phys. Rev. A* **53** 1349
[52] Dyubko S F, Efimenko M N, Efremov V A, Podnos S V, 1995 *Quantum Electronics* **22** 914
[53] Lorenzen C J and Niemax K 1983 *Physica Scripta* **27** 300
[54] Li W, Mourachko I, Noel M W, and Gallagher T F 2003 *Phys. Rev. A* **67** 052502
[55] Weber K H and Sansonetti C J 1987 *Phys. Rev. A* **35** 4650
[56] Snitchler G L and Watson D K 1986 *J. Phys. B: At. Mol. Phys.* **19** 259
[57] Miculis K, Beterov I I, Bezuglov N N, Ryabtsev I I, Tretyakov D B, Ekers A and Klucharev A N 2005 *J. Phys. B: At. Mol. Opt. Phys.* **38** 1811
[58] Hoogenraad J H, Vrijen R B, van Amersfoort P W, GvanderMeer A F, and Noordam L D 1995 *Phys. Rev. Let.* **75** 4579
[59] Fano U and Cooper J W 1968 *Rev. Mod. Phys.* **40** 441
[60] Beterov I I, Ryabtsev I I, Tretyakov D B, Bezuglov N N, Ekers A 2008 Sov. Phys. JETP **107** 20 http://arxiv.org/abs/0810.0339
[61] Allegrini M, Arimondo E, Menchi E, Burkhardt C E, Ciocca M, Garver W P, Gozzini S, Leventhal J J, Kelley J D 1988 *Phys. Rev. A* **38** 3271
[62] Browning P and Potter P E 1985 *An assessment of the experimentally determined vapour pressures of the liquid alkali metals, Handbook of Thermodynamic and Transport Properties of Alkali Metals* (Boston: IUPAC, Blackwell Scientific Publications) chapter 6.2.
[63] Boulmer J and Weiner J 1983 *Phys. Rev. A* **27** 2817

[64] Burkhardt C E, Garver W P, Leventhal J J 1985 *Phys. Rev. A* **31** 505
[65] Beterov I I, Tretyakov D B, Ryabtsev I I, Bezuglov N N, Miculis K, Ekers A, and Klucharev A N 2005 *J. Phys. B: At. Mol. Opt. Phys.* **38** 4349